Prebifurcation noise amplification and attractor hopping in an Erbium doped fiber laser

A dissertation submitted in partial satisfaction

of the requirements for the degree

Doctor in Sciences (Optics)

by

MSc Guillermo Huerta Cuéllar

Thesis advisor

Dr. Alexander N. Pisarchik

2009

Guillermo Huerta Cuéllar

2009

The dissertation of Guillermo Huerta Cuéllar is approved.

_____

Dr. Carlos Leopoldo Pando Lambruschini

_____

Dr. Vicente Aboites

_____

Dr. Alexander N. Pisarchik, Thesis Advisor

Centro de Investigaciones en Óptica A. C.

2009

To my mother . . .

who—among so many other things—

saw to it that I learned to touch-type

while I was still in elementary school

TABLE OF CONTENTS

List of Figures

vii

Acknowledgments/Agradecimientos

Primero, quiero agradecer al Dr. Alexander N. Pisarchik por haberme dado la oportunidad de trebajar con el y por el tiempo que ha dedicado a responder las dudas que se me han presentado, así mismo por el tiempo que me dedicó a pesar de que estubiera trabajando al momento que yo me presentará.

Agradezco también a mis sinodales, Dr, Yuri O. Barmenkov, Dr. Vicente Aboites y Dr. Carlos Pando Lambruschini, por sus importantes comentarios, correcciones y sugerencias para mejorar el presente trabajo de tesis.

A Adriana por su paciencia y que a pesar que que la situación de la distancia no fue muy favorable siempre me estubo apoyando y dando aliento para salir adelante con el trabajo que estaba realizando.

A mi madre que siempre se ha preocupado por mi bienestar y a pesar de muchas limitaciones siempre me ha apoyado para que siga adelante en lo que hago.

A mis amigos y compañeros Tonatiuh Rangel y Flavio Ruiz que me apoyarón mucho mientras he realizado mis estudios y con quienes he compartido muy buenos momentos en este ciclo.

A los doctores Donato Luna, Victor Castillo, Victor Pinto, Sergio Calixto, Bernardo Mendoza, Norberto Arzate, Carlos Perez, Ismael Torres y otros que en su momento tube la oportunidad de conocer, platicar y compartir consejos y/o sugerencias.

A mis amigos y compañeros Armando Gomez, Mariana Alfaro, Juan Carlos Ramirez, Diana Arroyo, Cornelio Alvarez, Trinidad Guillen, Jos Luis Cabellos, Guillermo Cardenas, Mario Wilson, Maria Doreen Alicia Martha Dignowity Wel-

Vita

1977   Born, San Luis Potosí, S. L. P, México.

1995–1997   Bachelor in Physics ans Mathematics.

1998–2002   Engineer in Physics (Optoelectronics), Faculty of Sciences, Autonomous University of San Luis Potosí (U.A.S.L.P.), with the thesis "Design and implementation of a back counter based in VHDL programing".

2002   Scientific summer in the Astronomical Institute of the Autonomus National University of México, (UNAM). Taking courses as Astrophysics, Interstellar Media, Galaxies, and Cosmology

2002–2004   Masters Degree in Aplied Sciences (Photonics), Instituto de Investigación en Comunicación Óptica, UASLP, with the thesis "Photoselective chemical etching in InAs and GaSb to manufacture microscopical lens for aplication in VCELS".

2006   Pre-doctrate stance in the *Consiglio Nazionale delle Ricerche - Istituto dei Sistemi Complessi*, Florence, Italy, working with the teme "Complex Networks: Structure and applications".

2005–2009   Doctorate in Apllied Sciences (Optics), Centro de Investigaciones en Optica, A. C. In León, Gto. México, with the thesis "Prebifurcation noise amplification and Attractor hopping in an Erbium doped fiber laser".

PUBLICATIONS

⋆ **G. Huerta–Cuellar**, Alexander N. Pisarchik, Yuri O. Barmenkov and Alexander V. Kir'yanov, "Pre–bifurcation noise amplification in a fiber laser", *Physical Review E*, **79**, (2009) 036204.

⋆ Guillermo Huerta–Cuellar, Alexander N. Pisarchik, and Yuri O. Barmenkov. "Experimental characterization of hopping dynamics in a multistable fiber laser", *Physical Review E* **78**, (2008) 035202(R).

⋆ **G. Huerta– Cuellar**, S. Guel Sandoval, F. De Anda Salazar, A. Garnache and A. Joullié. "Photoselective chemical etching of InAs and GaSb to manufacture microscopic mirrors". *Journal of Applied Electrochemistry*, **38**:269271, (2008).

⋆ F. Sorrentino, M. di Bernardo, **G. Huerta–Cuellar** and S. Boccaletti. "Synchronization in weighted scale free networks with degree-degree correlation", *Physica D.* **224** (2006) 123.

ABSTRACT OF THE DISSERTATION

Prebifurcation noise amplification and attractor hopping in an Erbium doped fiber laser

by

MSc Guillermo Huerta Cuéllar

Professor Dr. Alexander N. Pisarchik, Thesis advisor

Centro de Investigaciones en Óptica A. C., 2009

This thesis presents experimental results on stochastic and deterministic dynamics studies carried out in an Erbium doped fiber lasers (EDFL) which are presented to be compared with the results of numerical simulation using an advanced two-level laser model. The dynamics of this laser under external modulation is very rich; it can exhibit different bifurcations, chaos, and crises; furthermore, for different modulation parameters, one can encounter the coexistence of multiple periodic regimes (attractors).

In the experiments with EDFL we demonstrate a strong noise amplification in the vicinity of the critical points. Many are the situations in nature where this phenomenon can be experienced: heart strokes, eruptions, earthquakes, etc.

Another phenomenon studied in this thesis is the attractor hopping. As the noise added to a system is increased, the laser brings out different periodic states defining multistability zones. Then, as noise is augmented, more and more of these states come to form part of the hopping attractor. For certain input noise, when more and more states are involved in the hopping process, there is a little change in the output noise. Such a noise-independent regime can be promising for some important applications, in particular, detectors transparent to noise.

Resumen

Esta tesis presenta resultados experimentales de estudios sobre dinámica estocástica y deterministica realizados en una fibra láser dopada con Erbio (FLDE) los cuales se presentan para ser comparados con resultados de simulaciones numéricas usando un avanzado modelo de láser de dos niveles. Usando modulación externa, la dinámica de este láser es muy rica; puede exhibir diferentes tipos de bifurcaciones, caos y crisis; ademas, para diferentes parámetros de modulación se puede encontrar la coexistencia de múltiples regímenes periódicos (atractores).

En los experimentos con FLDE encontramos una fuerte amplificación de ruido cercana a puntos críticos. En la naturaleza, existen muchas situaciones en donde este fenómeno se puede observar: ataques al corazón, erupciones, terremotos, etc.

Otro fenómeno que se estudia en esta tesis es el atractor hopping. Cuando se añade ruido al sistema, el láser muestra diferentes estados periódicos los cuales definen unas zonas de multiestabilidad. Entonces, cuando el ruido se incrementa, más y más de esos estados aparecen para formar parte del atractor hopping. Para cierto valor de ruido agregado, cuando muchos estados están involucrados en el proceso hopping, el cambio del ruido a la salida es muy pequeño. Este régimen independiente de ruido puede ser prometedor para algunas aplicaciones importantes, en particular, para detectores transparentes al ruido.

INTRODUCTION

A thorough account of the experimental and some theoretical results in EDFL are given along with this thesis. The thesis contains Introduction, three chapters, and Conclusions.

Chapter one presents a fast review on laser nonlinear dynamics and its growing importance among researchers. The first three sections give a background on the chaos theory and introduce some important definitions. Lasers are described as dissipative systems, and, according to the material, each device is made of, a dynamical classification of lasers is given. In section 4, a simple laser theoretical model is introduced and variable elimination methods are used to define a laser based on both its material and its dynamics. In section 5, behavior, properties and types of attractors are illustrated to explain their coexistence. Bifurcations and pathways to chaos are described in section 7. A brief explanation of stochastic dynamics including stochastic resonance is given in section 8. A short account on EDFL performance is presented at the end of the chapter.

In chapter two is an introduction to the topic of prebifurcation noise amplification, followed by the setup description. Experimental results are provided to describe the dynamical processes in the EDFL. To end this chapter, a theoretical study and its results is compared with our experiment, and we underline how small the differences found are.

Chapter three gets to the core of hopping attractor theory, describes in detail the experimental setup used and thoroughly discusses the results. Some conclusions are given and the possibilities of future applications are presented.

Finally, some general conclusions are presented.

CHAPTER 1

Dynamics of lasers

1.1   Nonlinear dynamics in lasers

Interest in the field of dynamics of lasers is only a few years old [1, 2, 3], the stable continuously emitting laser having been at the center of attention for the last 50 years.

The interest is to a great extent motivated by the analogies of laser dynamics with dynamic chaotic and turbulent processes in other fields of the nature. On the other hand, it has become increasingly evident that the understood and "troublesome" laser properties such as unstable emission, poor reproducibility of laser pulses, limitation of attainable widths of ultrashort pulses and coherence lengths, and also problems with the emission mode pattern shapes, spontaneous irregular pulsing, etc., are not caused by insufficient technical skill, but are direct consecuences of the inherent nonlinear properties of lasers.

Apart from assisting in this respect, an undertanding of laser dynamics has helped in interpreting the rich phenomena of particular systems, that have been known for long time. A good example is the laser with an internal saturable absorber [4, 5]. In addition, it can lead to new useful applications, such as generation of phase coherent pulses in the infrared region, which combines the adventage of temporal compression of an averange power into high-power short

pulses with the coherence of continuos lasers.

Dynamics of lasers can be caused by the intrinsic properties of the laser systems [1], as in self pulsing, self-Q-switching lasers or trough external influences on the laser, such a time dependence of laser parameters, or interaction of external optical fields. Apart from the more practical questions of the conditions under which a particular laser system is stable, i.e. showing steady-state emission, or the conditions that will produce pulses in a possibly desired manner.

One of the most basic theoretical models of nonlinear dynamics (and fluid dynamics) is the Lorentz model which describes the simplest case of a laser, its dynamics is frecuently encountred in nature and also with lasers. This example give a taste of the mathematical treatment of non linear dynamics problems either through maps (discrete dymanics) or trough differential equations (time-continuous dynamics)[3].

1.2   Lasers as dissipative systems

Instabilities and chaotic motion occur in both conservative and dissipative systems. Whereas a conservative system never loses the memory of its initial conditions, dissipative systems have asymptotic solutions for $t \rightarrow \infty$ that can be independent of the initial conditions. This makes their treatment easier and simplifies their phenomenology. Lasers are dissipative systems: on the one hand energy is supplied to them by pumping, and on the other energy is dissipated via the out coupling of light and also relaxation processes, which include conversion into heat within the active medium. If the transients (i.e. the initial period required for the laser to forget its initial conditions, for instance after switching on or after crossing an instability point) are ignored, the laser can be described by

the asymptotic solutions ("attractors") (section 1.6) of its differential equations.

Lasers bear a resemblance to fluid flows. Energy can be supplied to a rectangular cell, containing a fluid, by a temperature difference between a bottom and upper sides. With a small temperature difference one observes heat conducton. In the laser case, this corresponds to pumping with a strength insufficient to reach the laser threshold. In the cell no macroscopic order occurs; the laser rids itself of the pump energy by radiating incoherent, unordered spontaneous emission.

With a larger temperature difference, circular macroscopically ordered flow patterns, or "rols", from spontaneously in the cell as a concequence of the transition from heat conduction to heat convection. In the laser this corresponds to pumping above threshold, where the spontaneous formation of spatially an temporally ordered (coherent) emission mode has taken place. The circular time-periodic motion in the convection cell may be thought as the counterpart of the oscillation at the optical laser frequency.

With an even larger temperature difference, the convection cell becomes turbulent as the laser at high pump strength becomes chaotic.

The equations describing in a simplified way both Bénard convection and the most elementary form of a laser are [6, 7]

$$\dot{x} = \sigma(x - y)$$
$$\dot{y} = x(r - z) - y \qquad (1.1)$$
$$\dot{z} = xy - bz$$

For the laser case x represents the electric field, y the polarization and z the population inversion. The meanings of the parameter b, r and σ for the two cases are as follows:

4

Bénard convection	Laser
σ:Prandtl number	$\sigma = \kappa/\gamma_\perp$
$r = R/R_c$	$r = \lambda + 1$
$b = \dfrac{4\pi^2}{\pi^2 + k_1^2}$	$b = \gamma_\parallel/\gamma_\perp$

Table 1.1: Meanings of the parameters b, r and σ for the Bénard convection and the simplest form of the laser.

where r is the Rayleigh number R normalized to the value that it takes at the onset of convection, k_1 is a dimensionless wavenumber, κ represents the damping rate of the laser resonator, λ is the pump rate above the threshold (λ=0 at the laser threshold), $\gamma_\parallel$ is the energy relaxation rate in the laser medium and $\gamma_\perp$ is the polarization relaxation rate. For λ=0 an instability is found that corresponds to onset of convection ($r = 1$) and continuous laser emission.

Two kinds of thresholds can be defined for a laser: "the first laser threshold", which corresponds to the well know threshold for the stable laser emission and is equivalent to a second-order phase transition, and the "second laser threshold", which gives rise to onset of unstable behavior.

The dynamics of lasers of even the simpest type are thus closely related to basic models of nonlinear dynamics and hence to a variety of phenomena observed in other disciplines of science. Weather, economic, social, chemical and biological systems nowdays appear to be governed by chaotic dynamics [7, 8, 9, 10]. In contrast to these, the laser is relatively a simple system and, unlike the large majority of them, it is possible with lasers to control they degrees of freedom. Studies of laser dynamics may therefore be expected to provide increasing insight into the dynamics of non-linear systems in general, by gradually progressing from the most "confined" to less and less "confined" cases. The results of the study of laser dynamics might therefore, apart from their practical interest, prove useful

for understanding complex phenomena that have so far not been understood.

1.3   Dynamical classification of lasers

Lasers are usually classified according to the material that provides optical amplification. This material determines largely the properties of the laser: the mode of operation (pulsed or continuous), the emission wavelength, the output power/energy and the coherence properties. Gases, liquids, and solids can provide optical amplification when properly excited. A new classification based on time scale considerations introduced by Arecchi et al. [11] opened a new look at lasers as dynamical systems and can be considered as one of the most important achievements in laser dynamics.

The laser transition of the amplifying material can be homogeneously broadened, i.e. light of certain optical frequency can interact with all atoms-molecules, all of them having the same resonance frequency. The homogeneous linewidth, Δ_{ν_H} is given by the medium relaxation rates:

$$\gamma_\perp + \gamma_\parallel = \pi \Delta_{\nu_H} \tag{1.2}$$

Where $\gamma_\parallel$ and $\gamma_\perp$ are the relaxation rates for inversion and polarization, respectively. Specifically, lasers operating in a single emission mode are usually described by three equations. The three relevant variables: field, population, and polarization, decay on very different time scales, which are given by the relaxation rates κ, $\gamma_\parallel$, and $\gamma_\perp$. If one of these constants is large compared with the others, the corresponding variables relaxes fast and consequently adiabatically adjusts to the other variables. The number of equations describing the laser is then reduced. Precisely, single-mode lasers were called class A, B, and C depending on whether,

after suitable adiabatic elimination of fast variables, the laser dynamics is ruled by one, two, or three equations, respectively.

The laser equations for a class A laser reduce to one. Therefore, only constant output solutions exist. For the class B lasers, oscillation of energy between field and inversion is possible and the equations yield relaxation oscillations. Class C lasers with their coupled dynamics of field, inversion and polarization can display undamped periodic or nonperiodic (chaotic) pulsing.

Thus, the following classification has been introduced [11].

Class A (e.g., He-Ne, Ar, Kr, dye): $\gamma_\perp \simeq \gamma_\parallel \gg \kappa$. One single nonlinear field equation remains that means stable coherent emission.

Class B (e.g., ruby, Nd:YAG, CO, CO2, semiconductor, fiber): $\gamma_\perp \gg \kappa \geq \gamma_\parallel$. Only polarization is adiabatically eliminated and the dynamics is ruled by two rate equations for field and population that allows for damped oscillations of the energy between field and inversion (relaxation oscillations).

Class C (e.g., He-Cd, He-Xe, far-infrared gas lasers): $\gamma_\perp \simeq \gamma_\parallel \simeq \kappa$. The complete set of three equations has to be used, hence Lorenz like chaos is feasible.

Class B lasers, however, show chaotic dynamics when they are externally influenced (parametric modulation, injection of external light, feedback, bidirectional ring cavity, or saturable absorber). Dynamical instabilities and chaos observed in experiments with a class-A multimode infrared He-Ne laser [12], a class-B loss-modulated CO_2 laser [1], and a class-C ammonia laser [13] have been properly understood and described mathematically in according with the above classification. Moreover, this classification scheme allowed one to predict dynamical behavior of new lasers depending on the relationship of the relaxation rates of their variables, e.g., later to refer fiber lasers to the class-B lasers.

From the nonlinear dynamics view point, experiments with lasers offer advantages over similar investigations with fluids. Since the basic oscillation is an optical frequency, all characterictic frequencies are very high. Hence the requirements for parameter stability for measuring the time-dependent behavior for the long periods necessary for quantitative investigations are easier to fulfill than in fluid experiments.

1.4 Nonlinear dynamical behavior: mathematical concepts

In this section is described, from the mathematical point of view, the general features that can be expected in nonlinear dynamic behavior. This can be applied to the study of the dynamics of different kinds of lasers.

1.4.1 Nonlinear differential equations

Any kind of laser can be described, with some simplifications, by means of coupled nonlinear differential equations involving first-order time derivates. Thus, in general we have to deal with equations such as

$$\frac{d\vec{x}}{dt} = F_{\vec{\mu}}(\vec{x}, t) \tag{1.3}$$

where the time-dependent vector $\vec{x} = (x_1, ..., x_n)$ represents the n dynamical variables describing the laser system, so that its evolution defines a "trajectory" or "orbit" of the system in the "phase space" defined by these variables. $F_{\vec{\mu}}$ describes the nonlinear coupling existing between the dynamical variables in a given kind of laser. In general $F_{\vec{\mu}}$ depends on several "control parameters" $\mu_1, ..., \mu_p$ that characterize each specific set of experimental conditions; this set of parameters is

designated by a vector $\vec{\mu} = (\mu_1, ..., \mu_p)$. When the function F does not explicitly depend on time, the system is called "autonomus":

$$\frac{d\vec{x}}{dt} = F(\vec{x}) \tag{1.4}$$

where the subscript $\vec{\mu}$ on F has been omitted for simplicity. Lasers are autonomus systems, except when a time-modulated external influence is introduced. Unless it is explicitly indicated.

Given an initial condition $\vec{x}(t = 0) = \vec{x}^0$, it is well know that equations such as eq. (1.4) have a unique solution. This means that trajectories in the phase space never intersect. The only exceptions to this rule are the "singular" points, at which several trajectories can eventually end (or begin).

A solution $\vec{x}(t)$ of eq. (1.4) with initial condition $\vec{x}(0) = \vec{x}^0$ is sometimes represented by means of a time evolution operator $\mathscr{F}^t$, which when applied to $\vec{x}^0$ gives the point $\vec{x}(t)$ reached by the system at time t:

$$\mathscr{F}^t(\vec{x}^0) = \vec{x}(t) \tag{1.5}$$

Lasers are "disipative systems", i.e. they have energy exchanges with a thermal bath or a large system with many degrees of freedom. Dissipation or internal friction has an important consequence for autonomous systems: any volume V in the phase space contracts along time evolution:

$$\mathscr{F}^t(V) < V, \qquad \text{for all } t > 0 \tag{1.6}$$

9

1.4.2 Adiabatic elimination of variables (Slaving principle)

From the theoretical point of view, the study of a specific laser system requires the analytical or, in general, numerical solutions of differential equation such as eq. (1.4) for many differet initial conditions and experimental conditions. In many cases this can be excessively large quantity of information to handle or understand. Therefore, methods or thechniques for reducing the amount of information or the number of degrees of freedom, in such a way that the basic features of the dynamical evolution be retained, are very useful in these cases.

An almost equivalent problem appears from the experimental point of view; it is usually impossible to measure or to deal with the complete temporal evolution of all the dynamic variables, and only partial information is recorded, which should also keep the basic dynamic features.

Here is briefly described one of the most often used reduction methods; the adiabatic elimination of variables.

Often, in equations such as (1.4), one or several of the control parameters μ_j influence in a very direct way the temporal evolution of particular dynamical variables. For instance, the Lorenz laser equations (1.3), the normalized field and population relaxation rates σ and b influence, respectively, the field and population variables x and z, thorough the terms $-x\sigma$ and $-bz$ appearing in the respective evolution equations $dx/d\tau$ and $dz/d\tau$. In these cases, i.e. when a control parameter μ_j influences the time evolution of a variable x_j through term $-\mu_j x_j$, the following behavior can occur. If this parameter is much larger than the remaining ones, the influenced variable x_j rapidly "loses" the memory of its history (i.e. of the values reached at the preceding times), in such a way rapidly adapts to (or "adiabatically follows") the instantaneous values reached by the

remaining variables, with an "adaptation speed" approximately proportional to μ_j. Hence a good simplification for solving eq. (1.4) within a given time scale (or time resolution) consists in equating to zero, for all t, the time derivatives corresponding to the variables ralaxing within a faster time scale than the given one, and introdicing the resulting algebraic equations into the remaining differential equations. In this way the number of independent variables or degrees of freedom are reduced ("adiabatic eliminition").

Since, under these conditions, the slowly evolving variables completely determine the evolution of the physical system, they are called the "order parameters". It is said that they "slave" the subsystems controlled by the fast variables. Indeed, when a few order parameters rule the time evolution of a large system with many degrees of freedom, it is a sure sign that a large degree of order has been reached. Lasers are typical systems where the "slaving principle" applies, as Haken has elegantly explained [2, 14].

1.5 Asymptotic behavior

1.5.1 Attractors: definition and properties

For dissipative systems any solution or trajectory can be divided into two parts: the initial transient regime and the final or asymptotic regime, which is located within an "attractor".

An attractor is a set of points in the phase space towards which trajectories eventually tend. Because an attractor is a basic concept for characterizing the asymptotic dynamic behavior in dissipative systems, precise mathematical definitions have been formulated (Guckenheimer and Holmes, 1983 [15]; Eckmann and Ruelle, 1985 [16]). Explained in simple terms, these definitions include four

basic points or conditions for a (compact) set A to be an attractor:

i) The neighborhood of A contracts, with time, towards A ("shrinking neighborhood").

ii) Any trajectory originating inside the atractor remains within it ($\mathscr{F}^t(A) = A$ for all t.)

iii) Any trajectory within the attractor goes trough all of it: for arbitrarily large values of t the trajectory passes arbitrarily close to any point of the attractor (recurence property).

iv) It is non descomposable: it cannot be split into two disjoint pieces each satisfying the preceding conditions.

Many different trajectories can eventually settle on a given attractor. The set of points in the phase space which evolve towards a given attractor constitute its "basin of attraction".

There is no limit to the number of attractors that can exist for a given dynamical system (usually the number is small, but some simple systems have an infinity of them). The basins of attraction may be complicated, even if the attractors are simple; they may interlace in almost inextricable manners, defining "fractal" boundaries.

"Repellors" can also be defined; these have the opposite meaning to that of the attractors. They are sets of points from which trajectories go away. Physically they are less relevant than attractors.

The contraction of volumes in phase space (see eq. (1.6)) confers a common and important feature to any attractor: its volume is zero. This means that the

dimension of an attractor is lower than that of the phase space. This property is useful for classifying the different kinds of attractors.

1.5.2 Kinds of Attractors

There is given a simple classification of attractors based only on their dimension and other most apparent features.

a. One and two dimensional phase spaces

For systems described by only one or two variables (let us call them 1-D or 2-D cases), the Poincaré-Bendixon theorem (Hirsch and Smale ,1974 [17]) reduce the possible kinds of attractors to only a few simple ones (see in Table 1.2).

	Fixed Points	Periodic orbits	Quasi-periodic attractors	Strange fractal chaotic	
1-D	Yes	No	No	No	No
2-D	Node, focus	Closed curves	No	No	No
3-D	Node, focus, ...	Closed curves	Closed surfaces	Yes	Yes
n-D	Node, focus, ...	Closed curves	Closed surfaces Closed manifolds (dim $m < n$)	Yes	Yes

Table 1.2: Simple schematic classification of attractors, for the different possible dimensions $(n - D)$ of the phase space $(n = 1, 2, 3, ...)$.

b. Three and higher-dimensional phase spaces: periodic and quasi-periodic attractors

The periodic attractors appearing in 3-D and n-D $(n > 3)$ phase spaces are generalizations of the previous ones. Fixed points and closed orbits obviously exist, but the last ones are not necessarily confined on a plane.

The next higher-order attractors are closer surfaces (or "two-dimensional man-

ifolds") (see Table 1.2). The simplest is a toroidal surface or torus, T^2, in a 3-D phase space (Fig. 1.1); it appears when the time evolution is doubly periodic, for instance, when the trajectories can be described through two variables, such as y_1 and y_2 in Fig. 1.1, whose time dependence is periodic, with respective periods T_1 and T_2:

$$y_i(t) = \frac{2\pi}{T_i}t \qquad (mod = 2\pi) \qquad (1.7)$$

Two cases may be distinguished. First, if T_2/T_1 is a rational number, then the trajectory is a closed line on the toroidal surface (see Fig. 1.1, for which $T_2/T_1=1/4$). In fact, in this case the attractor is not the toroidal surface but only the closed line. If the time evolution along this orbit is described through the phase space variables $x_i(t)$ (i=1,2 or 3), their Fourier spectra contain both frequencies $f_1 = 1/T_1$ and $f_2 = 1/T_2$ (and also, in general, any linear combination $lf_1 + mf_2$ where l and m are integers (positive or negative), if the periodic evolution is not exactly sinusoidal).

The other possible case is when T_2/T_1 is an irrational number (i.e. the periods T_1 and T_2 are incommensurate). The trajectory covers the whole toroidal surface and does not close (i.e. it does not reach the initial point) for any finite time t. In this case the trajectory is periodic in each of its cordinates y_1 and y_2, but there is not periodicity for the whole evolution (or it is "periodic" with a period $T \to \infty$); we are in the presence of a "quasi-periodic attractor", which is constituted by the toroidal surface (or, in general, by a two-dimensional manifold).

It might seem an unphysical refinement to distinguish between rational and irrational numbers for the ratio T_2/T_1, if one takes into acount experimental uncertainty. See for this aspect Bergé, Pomeau and Vidal (1984)[18], where the loking effect between two oscillators is considered.

The conclusions of this illustrative example can be easily generalized to phase
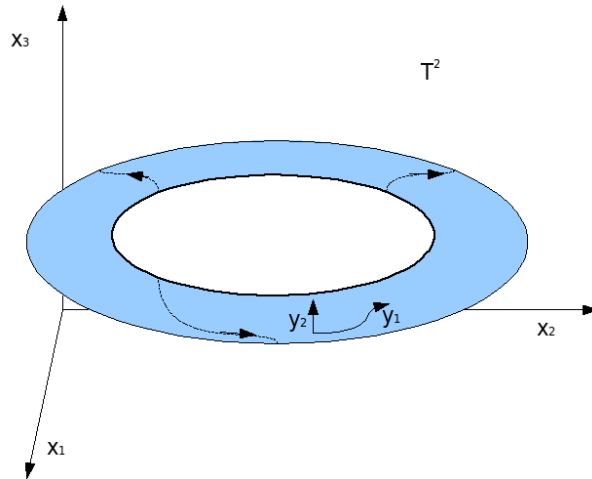
Figure 1.1: A two-dymensional in a 3-D phase space: a toroidal surface or torus T^2. y_1 and y_2 define a set of coordinates on the torus and the dashed line represents a periodic orbit on it.

spaces of any dimension $n \leq 3$: the periodic orbits can display from one- to $(n-1)$-fold periodicity, and the tori and "hyper-tori" T^n can have dimensions n' from 2 to $(n-1)$. The hyper-torus dimension indicates the number of different periods ruling the corresponding quasi-periodic dynamic behavior. In general, periodic and quasi-periodic attractors in an n-dimensonal phase space are m-dimensional closed manifolds, with $m < n$ (see Table 1.2).

c. "Strange" attractors

In n-dimensional phase space, with $n \geq 3$, attractors can exist that are not manifolds (i.e. smooth curves, hyper-surfaces, etc.) and do not describe periodic or quasi-periodic dynamic evolution. They are know as "strange" attractors, which means that they are "fractal" and "chaotic". A fractal attractor is characterized by the fact that its Hausdorff dimension is larger than its geometrical (or topological) one and usually is not an integer. Its origin lies in the intense

stretching and repeated folding in some directions during the volume contraction in phase space (see eq. 1.6), as is schematically illustrated in Fig. 1.2. Pictorically, the eventual "contract" between adjacent sheets of the folded surface confers some effective degree of "thickness" to the surface, so that, in the example in Fig. 1.2 its effective dimension can be in some sense larger than 2 (and lower than 3). This value is the fractal or Hausdroff dimension.
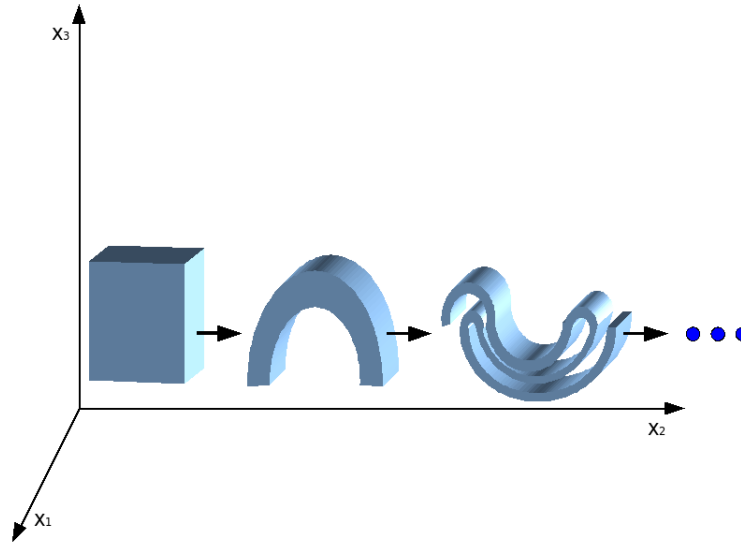
Figure 1.2: Volume contraction in phase space, as a result of the dynamic evolution. There are stretchings and foldings in some directions.

An attractor is called "chaotic", or equivalently, a system is behaving "chaotically", when it has a sensitive dependence on the initial conditions. This means that two orbits which initially are very close to each other exponentially separate; for long periods both remain within the attractor, but their initial proximity has been completely lost. The exponential separation takes place in the directions of stretching. It is said that any orbit in the attractor is "unstable within the attractor" (i.e. it is stable in the sense that it remains forever on the attractor).

Here is a reference to "deterministic" chaos, i.e. to that appearing in systems

16

with a finite number of degree of freedom or variables which are ruled by a finite set of differential equations, in such way that if one knows exactly the initial conditions, the future evolution can be exactly predicted. The point is that initial conditions can never be exactly know or repeated, so that the sensitive dependence on these conditions plays a basic role in the dynamic behavior of the system. It entails a loss of predictability over long periods.

The fractal character is more a geometrical than a dynamical property of an attractor, whereas the contrary for the chaotic character. All the chaotic attractors found up to now are fractal, but the contrary is not always true [8]. The invariance of an attractor under the dynamical evolution entails in general a phenomenon of "self-similarity": an enlarged view of a small zone of the attractor is similar to a larger zone of it.

1.6   Coexistence of attractors

Nonlinear dissipative systems often exhibit two or more dynamic equilibrium states for the same values of parameters. Some states may be chaotic while others are regular (periodic). Such multistability appears to be common for a variety of nonlinear systems. In a system with coexisting attractors a particular state is determined by initial conditions. The systematic organization of coexisting attractors allows one to predict the behavior of lasers, when initial conditions are allowed to evolve to their final states. Already in the beginning of the 1980s, the nonlinear behavior of various lasers was experimentally explored with respect to the emergence of coexisting states. The first experimental evidence of multistability in lasers has been demonstrated by Arecchi et al. [1] in a Q-switched CO_2 laser. Since then, it has been shown that lasers exhibit multistability due to pump modulation [19], loss modulation [20] or optical injection [21, 22]. Re-

cently, a rich variety of bifurcations and coexistence of multiple attractors which appear in the primary saddle-node bifurcations and their relation to main laser resonances have been demonstrated in a diode-pumped Erbium-doped fiber laser with pump modulation [23, 24, 25] (Fig. 1.8).
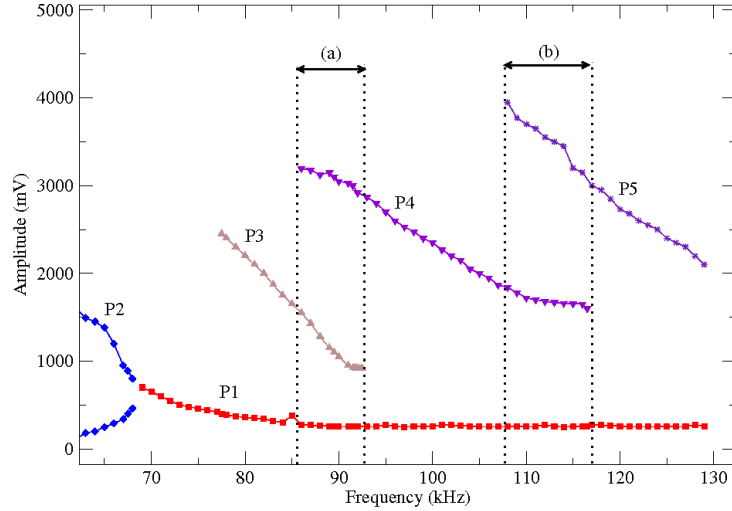
Figure 1.3: Bifurcation diagram in a fiber laser with pump modulation. For different modulation frequency we can observe, (a) coexitence of attractors P1, P3, and P4, and (b) coexistence of attractors P1, P4, and P5.

The dynamics in lasers with an optical feedback due to the reflection from a mirror often leads to delay differential equations introduced by Lang and Kobayashi in 1980 [26], where the delayed feedback is a source of the emergence of complicated behavior including multistability [27, 28]. Masoller [29] has shown that inevitable noise and in some cases a certain amount of external feedback results in complex hopping dynamics between different coexisting attractors in the system. For a particular range of noise amplitudes, this jumping exhibits a resonant behavior due to the interplay of the delayed feedback and the noise. The residence times probability distribution measuring the time spent by the trajectory in the neighborhood of an attractor exhibits peaks at multiples of the

18

delay time. The strength of the peaks reaches a certain maximum for an optimal noise level indicating the resonance. Laser physics provides also important technological problems which need to control multistability. One famous example is the so-called "green problem" [30] present in the operation of intracavity frequency-doubled Nd:YAG lasers. Usually, these lasers emit infrared light but using a nonlinear optical crystal, this light can be converted into visible green light. Unfortunately, this technique produces irregular fluctuations in the output intensity so that additional stabilization mechanisms like feedback control need to be applied to obtain a stable output [31]. The feedback control, however, induces multistability which can be tackled by the attractor annihilation method [32, 33] to make the system monostable. The method implies a harmonic perturbation leading to attractor destruction. This method has been realized experimentally first in a loss-modulated CO_2 laser [32] and then in a pump modulated fiber laser [34].

1.7 Bifurcations and roads to chaos

In general, a small variation in one or several laser parameters produces small (continuous) changes in the laser output, so that the system is said to be "structurally stable". However, for some specific parameter values one of the solutions (or attractors) may suffer a strong qualitative change. Such a behavior is called a "bifurcation" and the system is said to be "structurally unstable" for this parameter value. Very often when a control parameter is varied and a bifurcation appears at some critical value, it is followed by a sequence of new bifurcations at higher values of the parameter. Each new attractor appearing in the bifurcation chain is usually more complex than the previous one and eventually it becomes chaotic. The sequence is called a "road (or route) to chaos". The number of

types of routes to chaos is unknown but it has been observed that some of them appear very often, and for this reason they are called "scenarios". In the following subsection a brief description of the most important scenarios to chaos observed in lasers is presented.

1.7.1 Bifurcations

Next, are considered the most usual different kinds of bifurcations.

Local codimension-one bifurcations

A bifurcation is said to be "local" when the cualitative changes affecting the bifurcating solution can be analysed by studying only the region of the phase space close to the solution. Also a bifurcation is said to be "codimension one" when it satisfies the two following conditions: (i) it can be found by varyng only one (any one) of the control parameters of the system, and (ii) a continuous change, within a finite range, in any one of the remaining control parameters does not cause the bifurcation to disappear, but induces only smooth quantitative changes on the bifurcation features.

Here, there are considered two cases.

a. *Case of a fixed point*

A means of finding the possible bifurcation points affecting a fixed-point solution is to study its dynamical stability. If, when calculating the characteristic exponents as a function of a control parameter μ one finds that for some value of μ the real part of the exponents (or of a pair of complex conjugate exponents) changes from negative to positive values, it means that the stable fixed point becomes unstable and a new kinf of stable solution

probably sets in. By means of suitable change of variables, this kind of bifurcation can be described through only one real (or in some cases, complex) variable, which here is denoted as x; when this is done the problem is said to be reduced to the "normal form" (in general, the normal variable x corresponds to the direction of the eigenvector associated whit the characteristic exponent whose real part changes its sign).

Thaking as zero the values of the control parameters μ at which the bifurcation appears, and restricting the nonlinear terms of order up to 3, the simplest types of bifurcations are as schematically described in Table 1.3, where the bifurcation name the function F appearing in the differential equation $\dot{x} = F(x)$, and the "bifurcation diagram" showing the stable and instable branches of fixed-points solutions in the (μ, x) plane are represented. In the case of the Hopf bifurcation, the function F includes an arbitary constant c which does not play the role of a control parameter and the variable is complex $x = x_1 + ix_2$, so that in fact two real variables x_1 and x_2 are needed.

Table 1.3 shows only the "supercritical" or "nornal" bifurcations, in which the non-linear term contribution is opposite to that of the constant or linear term. By changing the sign of the non-linear term in the function F of Table 1.3 the "subcritical" or "inverse" bifurcations are found, the bifurcation diagrams on which are obtained by applying a transformation $(\mu, x) \rightarrow (-\mu, -x)$ to those in the Table 1.3 and (for the pitchfork and Hopf cases only) by changing the stability character of all the branches (stable $\leftrightarrows$ unstable).

b. *Case of closed orbit*

Name	F	Bifurcation diagram
Saddle-node (or tangent)	$\mu - x^2$	
Transcritical (or with stability exchange)	$\mu x - x^2$	
Pitchfork	$\mu x - x^3$	
Hopf	$(\mu + ic)x - x|x|^2$	

Table 1.3: Supercritical codimensional-one local bifurcations or fixed-points for a system $\dot{x} = F(x)$.

The fact that at bifurcation point the periodic orbit becomes unstable implies that a Floquet multiplier crosses the unit circle in the complex plane, which can take place in three ways:

(i) *Through the point +1.* In this case the results are very similar to the previous ones, allowing saddle-node, transcritical and pitchfork bifurcations. The function f defining the associated Poincaré return maps $x \rightarrow f(x)$ (or equivalently, $x_{m+1} = f(x_m)$) coincides with the corresponding function F in Table 1.3, except for the addition of a term x. For instance, for a saddle-node it is

$$f(x) = x + \mu - x^2 \tag{1.8}$$

(ii) *Through the point -1.* For this situation, no analogy with the fixed-point can exist. A "period doubling" or "subharmonic" or "flip" bifurcation appears, the bifurcation diagram of which looks identical with that of the pitchfork bifurcation of a fixed point, but the dynamics is different: the two parabolic branches do not correspond to independent solutions; instead, there is a unique solution whose return map alternates from one branch to the other indefinitely. In other words, the orbit closes at the second return instead of the first, so that its period becomes twice the original one. The normal form for the Poincaré map is

$$f(x) = (-1 + \mu)x - x^3 \tag{1.9}$$

In cases (i) and (ii) above, the variable x corresponds to the direction of the eigenvector associated with the Floquet multiplier +1 ans -1, respectively.

(iii) *Through a point $\xi \neq \pm 1$.* In this case two complex conjugate Floquet multipliers, ξ and ξ^*, cross the unit circle. The bifurcation is similar to a Hopf bifurcation and it is often know under the same name, but in fact there is one important difference: instead the circumference (corresponding to a limit cycle) appearing in the bifurcation diagram for $\mu > 0$ in the Table 1.3, the poincaré map now gives a series of points also located on a circumference but the order of appearance is such the angular distance from each point to the consecutive one is constant:

$$x \to f(x) = xe^{i2\pi\theta}, \qquad 0 \geq \theta > 1 \tag{1.10}$$

Thus, if θ is irrational, the whole circumference is covered, denoting quasi-

periodic behavior (the limit cycle has bifurcated to a toroidal surface T^2 but if θ is rational only a finite subset of points appears, which corresponds to a closed orbit on the toroidal surface. For $\theta = +1$ and -1, the previous cases (i) and (ii), respectively, are encountered.

Through a similar scheme, the torus T^2 could in turn bifurcate, for another value of the control parameter μ, to an hyper-torus T^3, and so on.

Crises

When a control parameter is varied and two solutions or attractors coalesce, a "crises" can occur, which consist in a sudden expansion, contraction or disappearance of the attractors. A typical example is a coalescence between a chaotic attractor and an unstable fixed point or periodic orbit, which leads to sudden changes in the chaotic attractor.

1.7.2 Roads to Chaos: Scenarios

A. Feigenbaum scenario (period-doubling road)

The most common route to chaos for class B lasers is the one through a sequence of subharmonic bifurcations which appear in the following way

$$T \rightarrow \mu_1 \rightarrow 2T \rightarrow \mu_2 \rightarrow 4T \rightarrow \mu_3 \rightarrow 8T \rightarrow \mu_4 \rightarrow \ldots \mu_\infty \rightarrow chaos \quad (1.11)$$

where $2mT$ ($m = 0,1,2,...$) represents the period of a closed orbit attractor and μn ($n = 1,2,3,...$) denote the critical values for the control parameter μ. This sequence known as the Feigenbaum scenario [13] was observed experimentally first in a loss-modulated CO_2 laser [1] and then in many other lasers of all classes. The typical time series corresponding to the

period-doubling route to chaos are shown in Fig. 1.4 (left-hand column) for a pump-modulated fiber laser, as the modulation frequency decreases.

The Feigenbaum scenarios can be also identified by looking at the power spectra (see right-hand column in Fig. 1.4). The period-doubling is clearly seen through the appearance of the first subharmonic of the modulation frequency f_m.
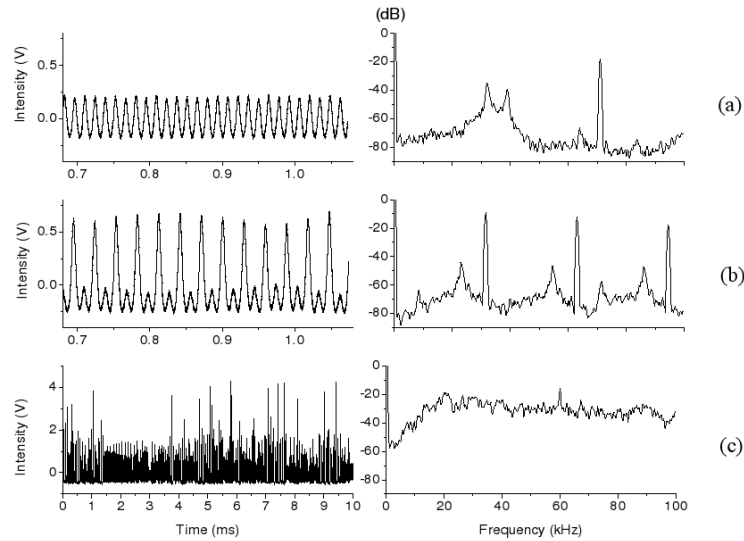
Figure 1.4: Period-doubling route to chaos with time series (left-hand column) and power spectra (right-hand column) in a pump-modulated fiber laser. (a) Period 1 at $f_m = 72$ kHz, (b) period 2 at $f_m = 63$ kHz, and (c) chaos at $f_m = 63$ kHz.

B. Ruelle-Takens-Newhouse scenario (quasiperiodicity road)

This scenario consists of a sequence of three Hopf bifurcations H_1, H_2, and H_3 at critical values μ_1, μ_2, and μ_3.

$$FP \rightarrow H_1(\mu_1) \rightarrow T \rightarrow H_2(\mu_2) \rightarrow T^2 \rightarrow H_3(\mu_3) \rightarrow T^3 \rightarrow \ldots chaos \quad (1.12)$$

As the diagram shows, the attractor is fixed point FP (or stable steady

state) for $\mu < \mu_1$; at $\mu = \mu_1$ it transforms into a periodic orbit T; at $\mu = \mu_2$ it changes again to a torus T^2 which entails a quasiperiodic behavior with two incommensurate frequencies, and at $\mu = \mu_3$ a new independent frequency appears, so that in principle a T^3 attractor (hypertorus) would be expected, but in many cases it is unstable towards some kinds of fluctuations and becomes chaotic. The Fig. 1.5 shows the bifurcation diagram of the peak intensity demonstrated the road to chaos through quasiperiodicity and Fig. 1.6 represents the corresponding time series.
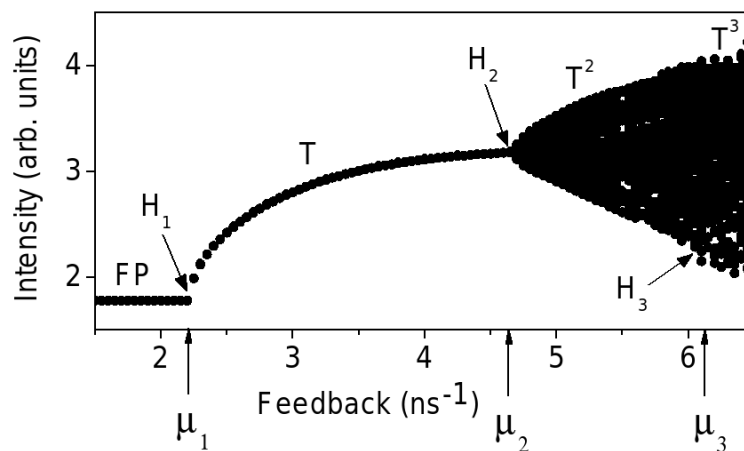
Figure 1.5: Bifurcation diagram of peak intensity of a semiconductor laser with external cavity with feedback strength as a control parameter.

The Ruelle-Takens-Newhouse scenario has been identified by observing the power spectrum of a dynamical variable, which is similar to the schematic example in Fig. 1.7. The broad-band spectrum corresponds to the chaotic dynamical evolution: some peaks are usually still apparent, that indicates that the previous periodic evolution has not completely disappeared.

The quasiperiodicity as a result of the interaction of three transverse modes has been observed first by Weiss et al. [12] in a multimode He-Ne laser and

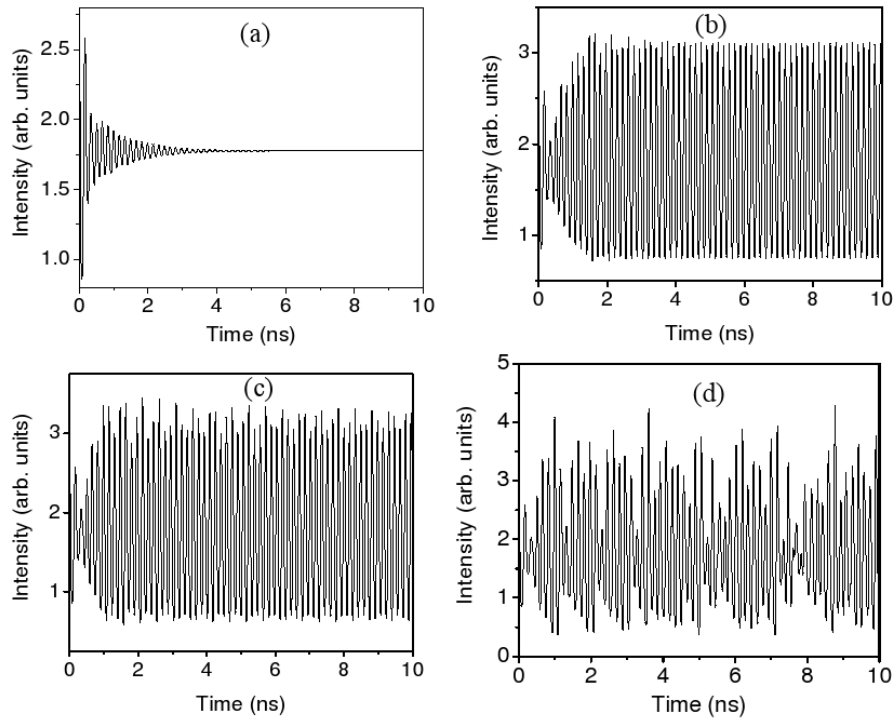Figure 1.6: Time series of laser intensity of a semiconductor laser with external cavity for different feedback strengths demonstrating (a) fixed point (FP), (b) periodic orbit (T), (c) quasiperiodic orbit (T^2), and (d) chaos (T^3)
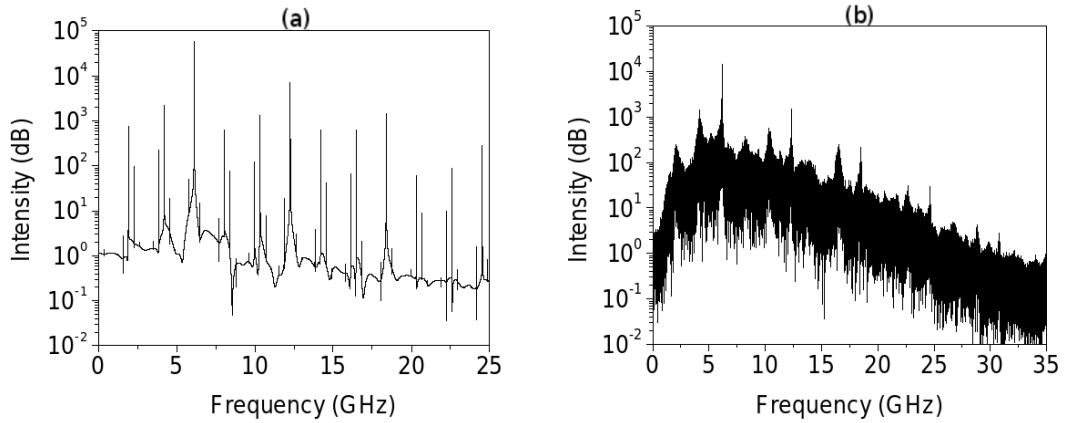
Figure 1.7: Power spectra of laser intensity corresponding to (a) quasiperiodic and (b) chaotic motions. Chaotic attractor has a broad-band spectrum.

by Biswas and Harrison [35] in a multimode CO_2 laser.

C. Intermittency scenario

The intermittency route to chaos is characterized by short, irregular (turbulent) bursts, interrupting the nearly regular (laminar) motion (Fig. 1.8). The duration of the turbulent phases is fairly regular and weakly dependent on control parameter μ, but the mean duration of the laminar phase decreases as μ increases beyond its critical value, and eventually they disappear. Hence only one bifurcation point is associated with the intermittency route to chaos.

Five types of intermittency have been observed in lasers: type-I, type-II, and type-III of Pomeau-Manneville intermittency [36], on-off [37], and crisis-induced intermittency [38]. A particular type of intermittency depends on the type of bifurcation at the critical point. The type-I and on-off intermittency are associated with saddle-node bifurcations, the type-II and type-III intermittency with Hopf bifurcation and inverse period-doubling bifurcation, respectively, and crisis-induced intermittency with crisis of chaotic attractors when two (or more) chaotic attractors simultaneously collide with a periodic orbit (or orbits) [10]. Quantitatively, intermittency exhibits characteristic interburst interval (laminar phase) statistics.

The type-I intermittency road to chaos has been found by Brun et al. [39] close to periodic windows in the chaotic domain in experiments with a linewidth-modulated nuclear magnetic resonance (NMR) ruby laser. They also observed sudden expansions of attractors, giving evidence of "crisis". The phenomenon "crisis" has been studied experimentally in more details with a loss-modulated CO_2 laser in the group of Glorieux [40]. The type-II intermittency route to chaos has been observed in a gain-modulated CO_2
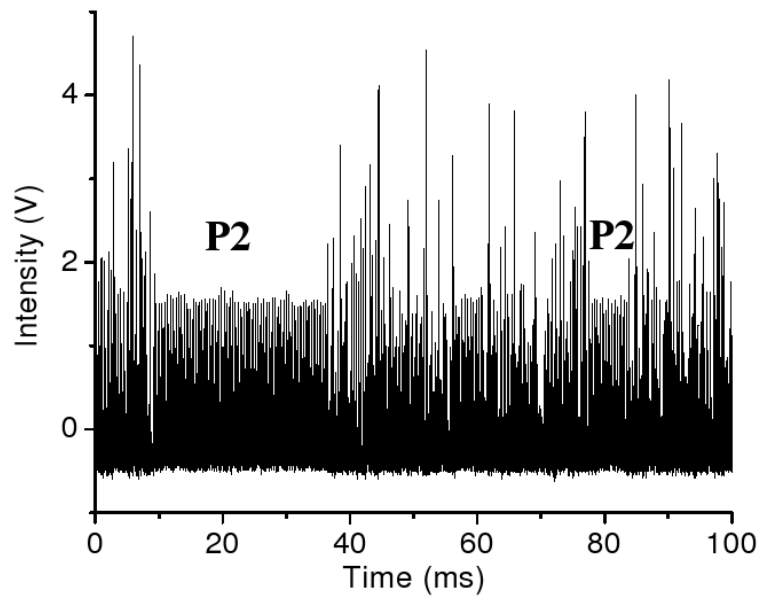
Figure 1.8: On-off intermittency in a fiber laser with pump modulation. The period-2 regime alternates at random times with the coexisting chaotic regime.

laser with cavity detuning [41] and in an external cavity semiconductor laser [42]. The type-III intermittency road to chaos has been found experimentally in an optically pumped FIR ring laser [43].

The mechanism for on-off intermittency relies on the time-dependent forcing (stochastic or periodic) of a bifurcation parameter through a bifurcation point, while the system switches between two or more unstable states, which are stable without external forcing. Instead, in Pomeau-Manneville intermittency and crisis-induced intermittency the parameters are static. Crisis-induced intermittency has been observed experimentally first in a NMR laser [44] and on-off intermittency in a semiconductor laser with external cavity [45].

1.8 Stochastic dynamics

It is commonly recognized that Einstein (1956) [46] established the theoretical foundation of stochastic calculus in his doctoral research and a series of papers on this subject, although Brownian motions, as a fundamental building block stochastic calculus. Since then, the literature on stochastic dynamics has been steadily increasing. This topic has been the topic in various subject areas including economy, finance, geology, ecology, population dynamics and biology. In the area of mechanical and civil systems, stochastics dynamics is known as random vibrations [47].

A schocastics process in an indexed set { X(t), $t \in T$ } of random variables X(t) defined on the same sample space Ω. t is the index parameter and T denotes the index set. In general, T can be discrete or continuous. Here is consedered the continuous random variable X(t) as stochastic process in function of time $t \in R^1$. An example of escalar stochastic process is the stress response at a critical point on a building during earthquake.

A continuous stochastic process X(t) essentially can be viewed as an infinite dimensional random vector. As in the case of n-dimensional random variables, the statics of the stochastic process is described by the *joint probability density* or *distribution functions* of the random variables in the process.

1.8.1 Stochastic resonance

Noise is generally associated with hindrance, with something that is irregular and cannot be perfectly controlled. Furthermore, noise is virtually unavoidable since it is impossible to isolate a system perfectly from its environment: all systems are interacting with their thermal reservoirs, which are a source of the

systems noisy dynamics. Even at zero temperature, when thermal (classical) fluctuations vanish, there is an interaction with zero-temperature reservoirs–a source of quantum noise [48].

Yet, addition of noise is sometimes able to make a nonlinear dynamical system behave more regularly. An intuitive picture of how such dynamics occurs in the overdamped motion of a classical particle with reaction coordinate $x(t)$ is the symmetric double well potential (Fig. 1.9).
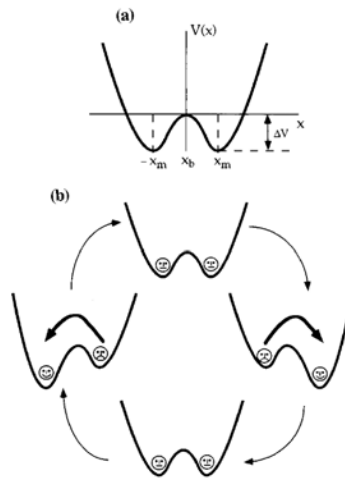
Figure 1.9: The fundamental mechanism of SR: in the prescence of an optimal level of noise, the stochastically actived transition between the two metastable states are most likely after one half-cycle of the periodic injected signal. Hence the response is optimally synchronized with the external modulation of the double well potential at nonvanishing noise strength

If this system was noise-free, the particle's motion would relax within the potential well where it was initially launched. Coupling to a thermal bath results in random kicks of the particle at random times so that eventually the particle can hop over the potential barrier–undergo a noise-assisted transition to the neighbouring well. The thermal activation rates, given by the famous Kramers formula [49], are functions of the ratio of barrier height to noise level. If a small

periodic modulation is applied to the potential at a modulation frequency much smaller than the intrawell relaxation rate, in itself unable to carry the particle deterministically across the potential barrier, the thermal activation rates are periodically modulated in time. Consequently, at a certain phase of the signal the probability of undergoing a transition to the neighbouring well increases, whereas the probability for the opposite transition is suppressed. If we now observe realizations of the stochastic process $x(t)$ for different noise strengths, we see that for some optimal, finite amount of noise, transitions between wells occur almost periodically in time. At that noise level, the timescale associated with the Kramers rate equals approximately half the signal period. This cooperative effect between a weak signal and noise in a nonlinear system, leading to an enhanced response to the periodic force, is termed *stochastic resonance* (SR).

1.9   Fiber Laser Doped with Erbium

Many different rare-earth elements, sucha as Neodimium (Nd^{3+}), Holmium (Ho^{3+}), Erbium (Er^{3+}), Tulium (Tm^{3+}), Iterbium (Yb^{3+}), Samarium (Ho^{3+}) and Praseodimium (Pr^{3+}) can be used to realize fiber amplifiers operating at different wavelengths in the range of 0.5-3.5 μm [50], some of them are show in Fig. 1.10. Erbium-doped fiber lasers (EDFL's) or amplifiers (EDFA's) have attracted the most attention because they operate in the wavelength region near 1.55 μ [51, 52, 53, 54]. Their development in wavelength-division multiplexing (WDM) systems after 1995 revolutionized the field of fiber-optic communications an led to lightwave systems with capacities exceeding 1 Tb/s.

The pumping at suitable wavelength provides gain throught population inversion. The gain spectrum depends on the pumping scheme as well as on the presence of other dopants, such germania and alumina, within the fiber core.
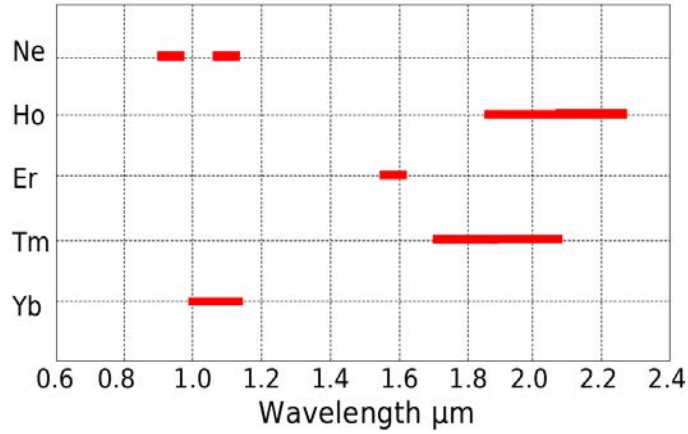
Figure 1.10: The red line shows the differnt wavelength range for some rare-earth fiber lasers.

Efficient pumping is possible using semiconductor lasers operating near 0.98 and 1.48 μm wavelengths.

The gain of an EDFL depends on a larger number of device parameter such as erbium concentration, amplifier length, core radius, and pump power [55, 56, 57]. In highly doped fibers, Er^{3+} ions tend to cluster in pairs [58] and that a fast cross-relaxation process takes place between doubly excited pairs [59]. This process was predicted to reduce the population inversion (i.e., higher threshold) and to compete with the pump-to-signal conversion process (lower conversion efficiency [59]). The percentage of pairs in each fiber is inferred from the data and shown to increase markedly with concentration.

CHAPTER 2

Prebifurcation noise amplification in a fiber laser

2.1 Introduction

The interaction between stochasticity and nonlinearity is a central current issue in studies in different dynamical systems, including radiophysical [60], climatic [61, 62], populational [63], geophysical [64], epidemical [65], and optical models [66, 67]. As a result of this interaction, noise, which is always present in a real system, can be amplified by the system while approaching a critical point. The idea that a system near the onset of a dynamical instability might be very sensitive to coherent or random perturbations came up in the works of Wiesenfield and McNamara [68, 69]. They have shown that time-periodic dynamical systems can greatly amplify small-amplitude perturbations in the vicinity of the simplest classes of codimensional-one bifurcations: saddle-node, transcritical, pitchfork, period-doubling, and Hopf. Latter, small-signal amplification near the period-doubling bifurcation was find out experimentally in a loss-modulated CO_2 laser [70]. According to the Wiesenfield's linear theory, prebifurcation noise amplification might be an effective diagnostic tool ("noise precursor") of a forthcoming bifurcation. It is of great practical importance to know how far the system is from a critical point. It was empirically observed that indeed strong changes

in noise amplification anticipate many oncoming natural and biological catastrophes, like tornado, earthquakes, convulsion of nature, epidemics, population extinction, myocardial infarction, etc., and thus it can serve as an indicator of the adverse natural phenomena and diseases. However, in natural and biological systems the parameters are usually uncontrollable and hence this effect cannot be studied systematically.

In this chapter experimental evidence of prebifurcation noise amplification in a real physical system is presented. The system under study is a diode-pump erbium-doped fiber laser with pump modulation. Natural noise is always present in the laser due to spontaneous emission and diode pumping. Moreover, additional noise can be added from an external noise generator. We find that noise fluctuations are amplified not only in the vicinity of a period-doubling bifurcation as was already shown in some theoretical papers, but also near saddle-node and crisis points [71]. It seems that this phenomenon is quite general and can be expected for other kinds of bifurcations in many dynamical systems. Numerical simulations on the base of the advanced laser model display good agreement with experimental results [71].

The analysis of prebifurcation noise amplification was performed using both linear [68] and nonlinear theories [72, 73, 74, 75]. The linear theory displays an infinite growth of perturbations, while the system approaches the bifurcation point [68], whereas the nonlinear theories demonstrate a saturation effect near the period-doubling [72, 73, 74] and pitchfork bifurcations [73, 64]. The theoretical analysis showed that the real part of one of the negative Lyapunov exponents becomes positive when the system approaches the bifurcation point [72]. According to the Wiesenfeld's theory [68], prebifurcation noise amplification can serve as noise precursor of bifurcation in a nonlinear system. The addition of white noise

gives rise to new broadband peaks not present in the noise-free system [68, 76]. These noise precursor peaks are centered at the new frequencies that appear only after the bifurcation. Noisy precursors of the period-doubling bifurcation have been observed in experiments on a semiconductor laser [67].

In this work the experimental evidence of prebifurcation noise amplification is provided. The experiments are carried out with a fiber laser subject to periodic modulation of the diode pumping. It is well-known that any laser has intrinsic noise due to the spontaneous emission of radiation. In this way is studied how this inherent laser noise and additional Gaussian noise applied to the diode pump current become apparent in the fiber laser power spectrum near saddle-node, period-doubling, and crisis bifurcations. Also this phenomenon was numerically studied with our improved laser model and the results of numerical simulations and the experimental ones are compared.

In Section 2.2 the experimental setup and the phenomenon of prebifurcation noise amplification in the vicinity of the saddle-node, period-doubling, and crisis points are obtained experimentally. The theoretical model of the erbium-doped fiber laser and the results of numerical simulations is presented in Section 2.3. Using the obtained results is demonstrated the validity of this model by comparing some important laser characteristics obtained numerically and experimentally. Finally, the main conclusions of the experiment are given in Section 2.4.

2.2   Experiment

A diode-pumped erbium-doped fiber laser (EDFL) is a commercial optical device. Due to its excellent optical properties (high gain and single-mode operation), EDFL is widely used as a light source for optical communications, reflectometry,

sensing, medicine, etc. [51]. On the other hand, EDFL is a complex dynamical system, which serves as a paradigm for studying many nonlinear dynamical phenomenon, such as bifurcations, chaos, frequency locking, and multistability [77, 24, 78, 79, 23, 80, 81, 23]. This laser belongs to class-B lasers [82], along with solid-state, semiconductor, and CO_2 lasers. In the lasers of this type, the polarization relaxation process is very fast and hence it is adiabatically eliminated, so that the dynamics are described by only two rate equations, for the laser field and for the population inversion.

2.2.1   Experimental setup

We used a 1560-nm EDFL subject to harmonic modulation of a 976-nm diode pump laser (Fig. 2.1). The 1.5-m Fabry-Perot laser cavity is formed by an active heavily-doped (2300 ppm) erbium fiber of a 70-cm length and 2.7-μm core diameter and two fiber Bragg gratings with a 1-nm FWHM (full width on half-magnitude) bandwidth, having 91% and 95% reflectivities for the laser wavelength (λ=1560 nm). The fiber laser output power is recorded, after going through a wavelength-division multiplexing coupler, with a photodetector and analyzed with an oscilloscope and a Fourier spectrum analyzer. The diode laser output power depends linearly on the laser diode current. In the experiments the diode current is fixed at $I = 69$ mA corresponding to the pump power $P = 18$ mW. The harmonic signal, $A\sin(2\pi f_m t)$ (A and f_m being the amplitude and frequency of the external modulation, respectively) from a signal generator and additive Gaussian noise $n\xi$ (n and ξ being the external noise amplitude and a random generated number, respectively) from a noise generator are both applied simultaneously to the diode pump current.

Without external modulation ($A = 0$), the fiber laser exhibits small-amplitude

Figure 2.1: Experimental setup.

oscillations (1-2% of the magnitude of the steady-state power) at the relaxation oscillation frequency f_r which depends on the pump power and noise as shown in Fig. 2.2. The appearance of this frequency in the spectrum is due to the diode pump laser intrinsic noise [83] and the fiber laser spontaneous emission. One can see that the additive noise slightly increases f_r. In our experiments we choose the laser parameters so that the relaxation oscillation frequency $f_r = 30$ kHz in the absent of external noise. Also, in the figure 2.2 it is ploted the numerically calculated dependence in the absence of the external pump modulation and noise, EDFL dynamics is ruled mainly by the following processes, explained in secc. 2.3: (i) the resonant ground-state absorption (GSA) saturation, (ii) the excited sate absorption (ESA) loss and cooperative effect of Auger up-conversion [84], both determined by the Er^{3+} ion energy levels' structure, and (iii) the amplified spontaneous emission (ASE).
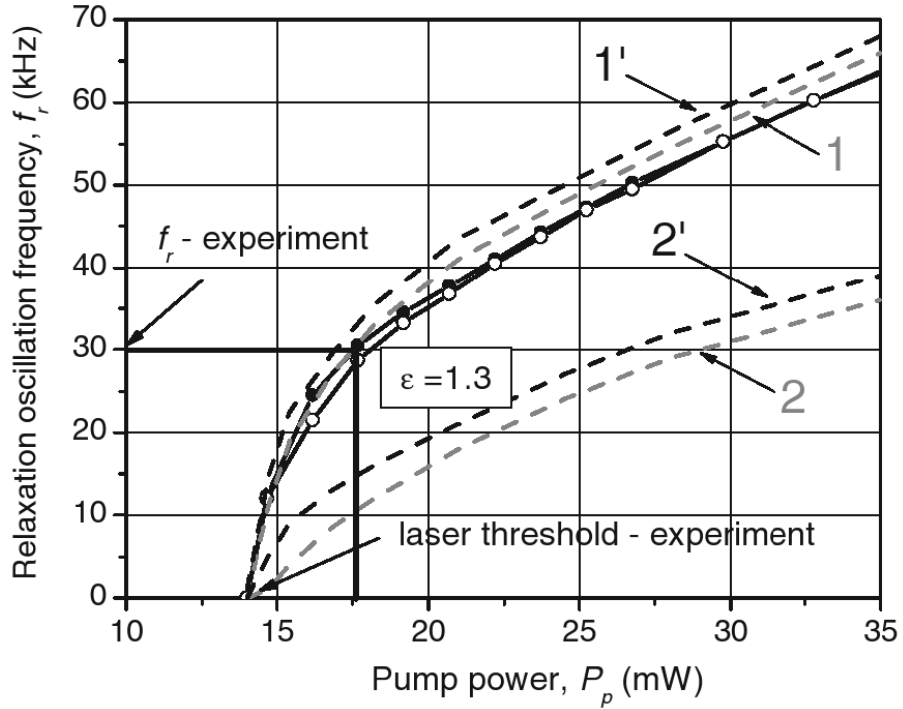
Figure 2.2: Experimental (solid lines) and numerical (dashed lines) dependences of EDFL relaxation oscillation frequency on pump power. The experimental curves are obtained with intrinsic laser noise (open dots) and with 50%-modulation depth external noise (filled dots). The theoretical curves 1 and 1' are calculated taking into account ASE and the curves 2 and 2' without ASE. The curves 1 and 2 are obtained in the presence of noise and the curves 1' and 2' without it. The calculated f_r with ASE coincides with the experimentally measured one (at $\varepsilon = 1.3$).

2.2.2   Experimental results

Figure 2.3 shows the experimental bifurcation diagram of the peak-to-peak laser intensity with the modulation frequency f_m as a control parameter for $A = 8$ dB and $n = 0$. One can see the coexistence of different periodic and chaotic attractors for certain modulation frequencies at left and also is showing at rigth sade, the experimental bifurcation diagram of the noise level in the frequency spectrum at the modulation frequency. This diagram was measured by taking different initial conditions which are changed by switching on and off the signal generator or by increasing and decreasing f_m. As was mentioned in some previous papers [77, 24, 78, 79, 23, 80, 81], EDFL dynamics, as well as the dynamics of other class-B lasers, is related to the main laser resonance, which appears close to f_r. The period-3, period-4, and period-5 attractors are born and dead in the saddle-node bifurcations. It is also seen the period-doubling and crisis bifurcations at $f_m \approx 68$ kHz and 60 kHz, respectively.

In this work we are interesting in the following question: How does the laser system amplify intrinsic and additional external noise near different bifurcations? The noise level of EDFL is measured in the power spectra of the laser intensity. The examples of such spectra for the period-3 attractor for two different modulation frequencies are shown in Fig. 2.4. One can see that the noise (ground) level for $f_m = 78$ kHz is higher than that for $f_m = 83$ kHz. This fact indicates that the laser amplify the noise while f_m approaches the saddle-node bifurcation which occurs close to 78 kHz (see Fig. 2.3). The similar behavior is observed in the vicinity of other bifurcation points.

Figure 2.4 shows the noisy spectral component N_m at the modulation frequency as a function of f_m for intrinsic laser noise [Fig. 2.5(a)] and for additive Gaussian noise $n = 200$ mV [Fig. 2.5(b)]. In both cases, prebifurcation noise
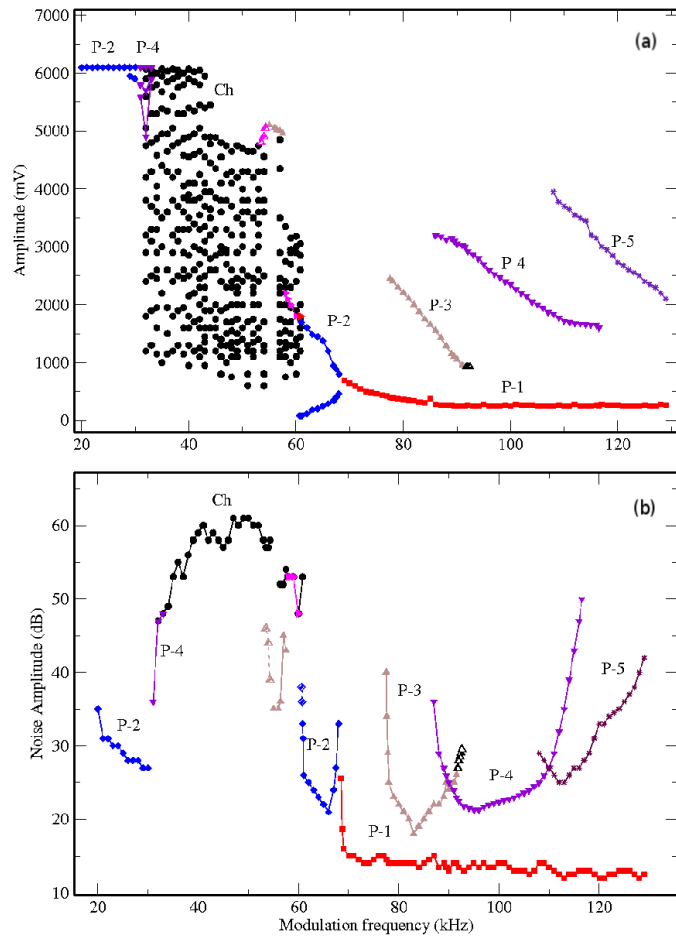
Figure 2.3: Bifurcation diagram. (a) in temporal series and, (b) noise level at the modulation frequency.
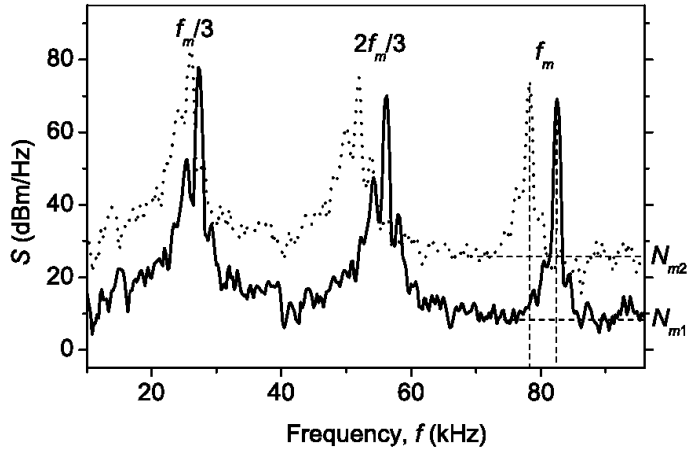
Figure 2.4: Comparison of experimental power spectra between f_m=78 kHz (near bifurcation) and, f_m=83 kHz (far of bifurcation).

amplification is evident near every critical point (saddle-node, period-doubling, and crisis). The closer the system to the bifurcation point, the stronger the amplification. The effect is more pronounsed at the correponding subharmonic frequencies for each attractor, i.e. at $f_m/3$ for P3, at $f_m/4$ for P4, and at $f_m/5$ for P5. Near the period-doubling bifurcation, the amplification is higher for smaller noise. The later is in good agreement with previously observed small-signal amplification [69, 70]. As seen from Fig. 2.4, the noise amplification near saddle-node and crisis bifurcations can reach 30 dB, i.e. the noise amplitude is increased by 3 orders of magnitude while approaching the critical point.

The later is in good agreement with previously observed small-signal amplification [69, 70]. As seen from Fig. 2.4, the noise amplification near saddle-node and crisis bifurcations can reach 30 dB, i.e. the noise amplitude is increased by 3 orders of magnitude while approaching the critical point.
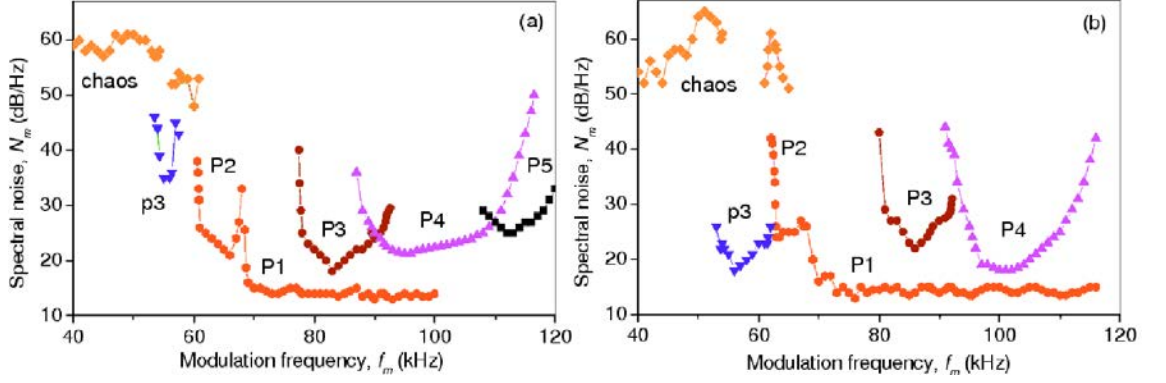
Figure 2.5: Noise amplification.

2.3 THEORY

2.3.1 Model

The main ideas underlying the model equations for EDFL have been developed in the previous works (see, for instance,[79, 23, 81]). In the absence of the external pump modulation and noise, EDFL dynamics is ruled mainly by the following processes (Fig. 2.6): (i) the resonant ground-state absorption (GSA) saturation, (ii) the excited sate absorption (ESA) loss and cooperative effect of Auger up-conversion [84], both determined by the Er^{3+} ion energy levels' structure, and (iii) the amplified spontaneous emission (ASE), an essential feature of a fiber laser with a long cavity. The periodic and stochastic pump modulations are introduced into the model as "external" disturbance factors which considerably affect upon EDFL dynamics.

For an easy EDFL modeling, a simplified two level model of Er^{+3} is used, and also only a point of the laser is applied to make a resaonable simulation time [83]. The balance equations for EDFL generation intracavity power P_g (in s^{-1}) and dimensionless population y of the upper laser level of Er^{3+} ($^4I_{13/2}$) are written as
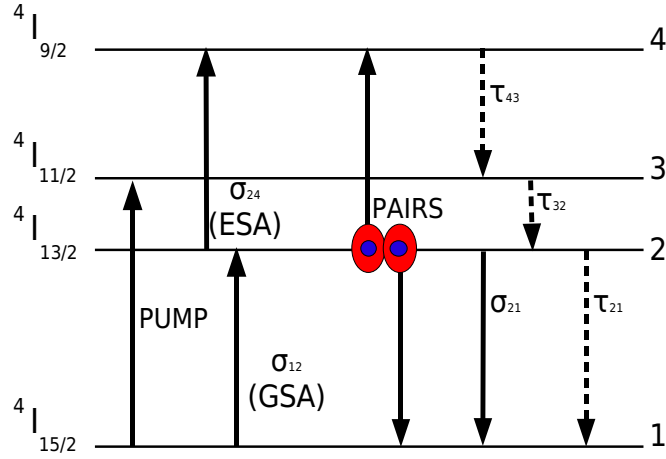
Figure 2.6: Simplified energy level diagram of Erbium.

follows

$$\frac{dP_g}{dt} = \frac{2L_0}{T_r}[P_g\{\Gamma\alpha_0[(\xi - \eta)y - 1] - \alpha_I\} + \Gamma\alpha_0(\xi - 1)y\mu\Delta\nu_{Er}K(y)exp(-L\gamma)]$$

(2.1)

$$\frac{dy}{dt} = -\frac{\Gamma\alpha_0}{N_0 S_a}P_g(y\xi - 1) - \frac{y}{\tau_0}\{1 + 4[K^*(y) - 1]\frac{\Gamma\alpha_0(\xi - 1)\tau_0\Delta\nu_{Er}}{N_0 S_a}\} - \frac{y^2}{\tau_1} +$$
$$\frac{1 - exp[-\delta\alpha_0 L_0(1 - y)]}{S_p N_0 L_0 h\nu_p}P_p[1 + A\sin(2\pi f_m t) + n\zeta]$$

(2.2)

where $\alpha_0 = N_0\sigma_{GSA}$ and $\alpha_0^* \approx 2\alpha_0$ are the small-signal absorption coefficients of the active erbium-doped fiber core at the generation wavelength λ_g and on the Er^{3+} emission band maximum at $\lambda^* \approx 1.53$ μm), N_0 is the Er^{3+} concentration, $\xi = 1 + \sigma_e/\sigma_{GSA}$ and $\eta = \sigma_{ESA}/\sigma_{GSA}$ are the coefficients addressing the relations

between the GSA, ESA, and gain cross-sections at λ_g (σ_{GSA} and σ_e being the cross-sections of the GSA and gain transitions between the $^4I_{15/2}$ and $^4I_{13/2}$ states and σ_{ESA} is the effective ESA cross-section in Er^{3+}); τ_0 is the lifetime of single Er^{3+} ions in the excited $^4I_{13/2}$ state; τ_1 is the effective relaxation time of the Er^{3+}-Er^{3+} pair clusters, where each Er^{3+} ion forming a pair is in the excited state; $\Gamma = 1 - \exp[-2(a/w_0)^2] = 1 - \exp(-S_a/S_w)$ is the overlap factor ($S_a = \pi a^2$ and $S_w = \pi w_0^2/2$ that indicate the part of the power of the fundamental fiber mode propagating through the fiber core, where a and w_0 are the core and beam radii); $T = 2n_0 L/c$ is the photon intracavity round-trip time, where L is the total cavity length being the sum of the active fiber length L_0 and the total length l_0 of all other intracavity fiber components, n_0 is the refractive index of silica, and c is the velocity of light in vacuum; $\alpha_l = \gamma - \ln(R_1 R_2)/2L$ is the intracavity overall losses, where γ stands for the total non-resonant intracavity losses and R_1 and R_2 are the reflection coefficients of the FBG couplers forming the EDFL cavity); $\Delta\nu_{Er}$ is the Er^{3+} emission bandwidth (assumed to be homogeneously broadened); δ is the dimensionless coefficient accounting for the ratio of absorption coefficient of erbium-doped fiber at the pump wavelength λ_p to that (α_0) at the generation wavelength λ_g; $\mu = \Delta\nu_g/\Delta\nu_{Er}$ is the factor addressing the ratio of the generation and spontaneous emission bandwidths; $h\nu_p$ is the pump energy quanta; and S_p is the pump radiation geometrical cross-section (it is assumed further that the pump radiation is effectively absorbed within the active fiber core: $S_p = \pi w_p^2 \approx S_a$); P_p (in W) is the pump power at the active fiber entrance.

The parameters responsible for periodic and stochastic external modulation are defined as follow. A and f_m are the amplitude and frequency of sinusoidal modulation, n is the Gaussian noise amplitude, and ζ is a random number ($A, n, \zeta \in [0, 1]$). The quantities K and K^* are the length-averaged ASE co-

efficients defined as

$$K = \frac{\exp\{L_0\Gamma\alpha_0\left[(\xi-\eta)\,y-1\right]\}-1}{L_0\Gamma\alpha_0\left[(\xi-\eta)\,y-1\right]}, \tag{2.3}$$

$$K^* = \frac{\exp\{L_0\Gamma^*\alpha_0^*\left[(\xi^*-\eta^*)\,y-1\right]\}-1}{L_0\Gamma^*\alpha_0^*\left[(\xi^*-\eta^*)\,y-1\right]}. \tag{2.4}$$

The asterisks mean the corresponding average values within the $\Delta\nu_{Er}$ range. For simplicity here we assume $\xi^* = \xi$, $\eta^* = \eta$, and $\Gamma^* = \Gamma$. Thus, the terms $2\Gamma\alpha_0(\xi-1)y\mu\Delta\nu_{Er}K(y)\exp(-L\gamma)$ in Eq. (2.1) and the term $4[K^*(y-1)][\Gamma\alpha_0^*(\xi-1)\tau_0\Delta\nu_{Er}]/(N_0S_a)$ in Eq. (2.2) characterize respectively the roles of ASE in establishing (seeding) generation in the laser cavity and the increasing rate of the laser upper level depopulation. The parameter values either measured experimentally or provided by fiber manufacturers are presented in Table 1.

λ_g	λ_p	$h\nu_p$	α_0	N_0	δ	$h\tau_0$
$1560nm$	$976nm$	$2.037x10^{-19}J$	$0.06cm^{-1}$	$2.4x10^{19}cm^{-3}$	0.7	ms
τ_I	η	σ_{GSA}	ω_0	$\Delta\nu_{Er}$	μ	ξ
ms	0.24	$2.48x10^{-21}cm^{-2}$	$2.61\mu m$	$25nm$	10^{-3}	2.25
a	Γ	γ	L_0	l_0	R_1	R_2
$1.35\mu m$	0.417	$8.7x10^{-4}cm^{-1}$	$0.82m$	$3.51m$	1	0.91

Table 2.1: Parameters used in numerical simulations.

2.3.2 Numerical results

In order to check the validity of our model Eqs. (2.1) and (2.2) and to ensure that the selected parameters (Table 1) correspond to the real experimental parame-

ters, we calculate the dependences of the relaxation frequency f_r on the pump power P_p without external modulation ($A = 0$) for four different cases (with and without accounting for ASE in the presence and absence of noise) and compare with the experiment (Fig. 2.2). A comparison of the presented theoretical dependences with the experimental ones allows one to reveal the importance of the ASE contribution. Only the account of ASE (curves 1 and 1', Fig. 2.2) allows the coincidence of the numerically calculated f_r with the experimentally measured value ($f_r \approx 30$ kHz) for the same excess over the laser threshold ($\varepsilon \approx 1.3$). Note, that the theoretical value for the EDFL threshold (near 14 mW) is remarkably close to its experimental value as well. When ASE is ignored (curves 2 and 2'), the difference from the experiment is very high. It is also remarkable that the theoretical dependences $f_r(P_p)$ for no noise ($n = 0$) and pronounceable ($n = 0.5$) noise almost coincide with the experimental curves (compare the curves 1 and 1' with the experimental data shown by the open and closed dots in Fig. 2.2); the additive noise slightly increases f_r. This coincidence proves the validity of our model and ensures its further application for the case of external pump modulation.

Next, we perform the temporal and spectral analyses of the time series of the intracavity laser power $P_g(t)$ calculated with Eqs. (2.1) and (2.2) for different amplitudes A and frequencies f_m of pump modulation and different noise levels n for fixed excess ε of the pump power over the first laser threshold. Figure 2.7 shows the power spectra of the EDFL intensity for two different modulation frequencies, $f_m = 83$ kHz and 78 kHz, and fixed $\varepsilon \approx 1.3$ ($P_p \approx 18$ mW), modulation depth (25%), and input noise amplitude (25%), when the laser works in the period-3 regime. One can see that the noise levels (output noise) at f_m and its third subharmonic $f_m/3$ are higher for $f_m = 78$ kHz than for $f_m = 83$ kHz, i.e. the laser amplifies noise while approaching the saddle-node bifurcation where the
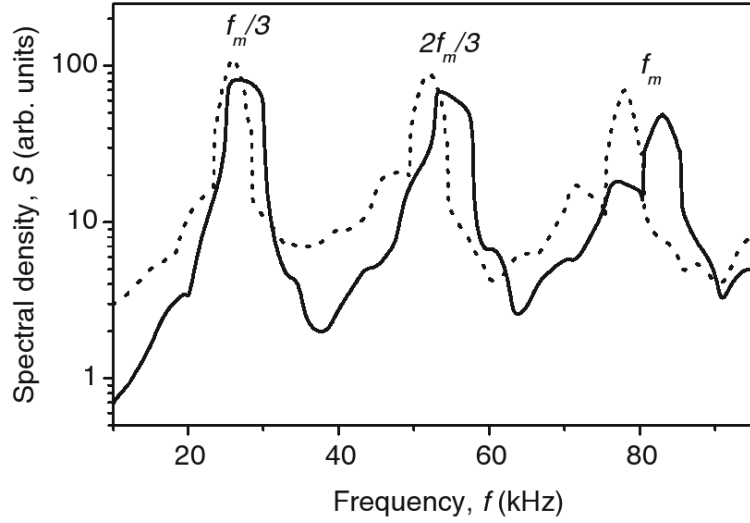
P3 attractor is born.

Figure 2.7: Numerically calculated power spectrum. Dotted points for f_m=78 kHz, and straight line for f_m=83 kHz

The numerical bifurcation diagram of the pump-modulated EDFL is similar to those already presented in several papers [24, 78, 79, 81, 23]. We should only note, that it almost coincides with the experimental diagram shown in Fig. 2.3.

Figure 2.8 shows the noise amplitude N_m at the modulation frequency f_m in the power spectrum as a function of f_m for different coexisting attractors (period 1 (P1), period 3 (P3), and period 4 (P4)). As in the experiment (Fig. 2.5), we observe significant noise amplification when the laser approaches a bifurcation point. One can see good agreement between the theoretical "noise bifurcation diagram" and the measured one (shown in Fig. 2.5). So, the conclusion made above, at analyzing the experimental results concerning an increment of "noisy" background of the EDFL with external modulation at approaching any of the bifurcation points (either saddle-node or period-doubling), is fairly supported by
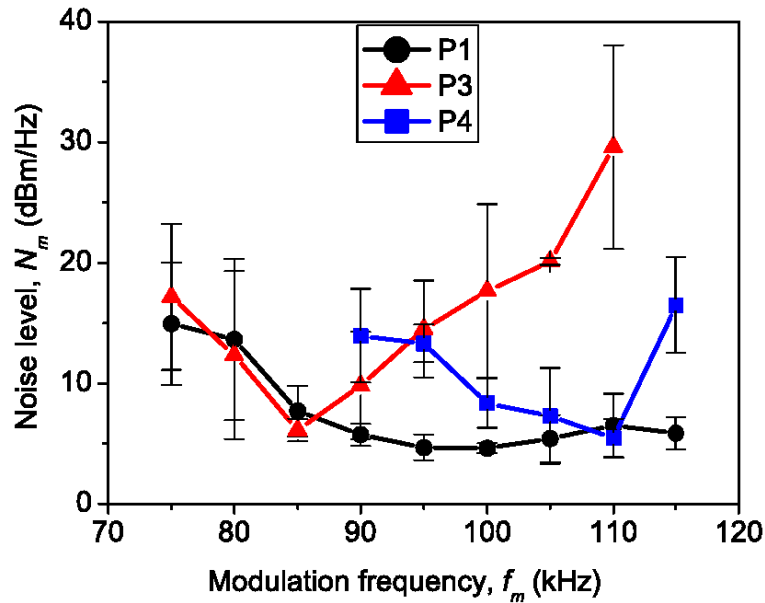
Figure 2.8: Calculated noise amplification.

the developed EDFL modeling.

2.3.3 Conclusions

In this chapter the experimental evidence of prebifurcation noise amplification near different types of bifurcations (saddle-node,period-doubling, and crisis) is demonstrated. The experiments have been carried out with a pump-modulated erbium-doped fiber laser with additive noise applied to the current of the diode-pump laser. The closer the system to the bifurcation point, the stronger noise amplification. The noise amplitude can increase by 3 orders of magnitude, while the system approaches saddle-node and crisis points. Near a period-doubling bifurcation, the effect is more pronounced for smaller noise. The results of numerical simulations with the advanced laser model demonstrate good agreement with the experiment. The comparison of the numerical results with the experi-

mental ones, also indicates the importance of the amplified spontaneous emission (ASE) to be taken into account in simulations of EDFL.

Many theoretical works indicate on generality of prebifurcation noise amplification. We beleive that this phenomenon can be also observed in experiments with other dynamical systems, for example, by analyzing meteorological and geophysical experimental data, that would be useful for prediction of oncoming catastrophes.

CHAPTER 3

Experimental Characterization of Hopping Dynamics in a Multistable Fiber Laser

3.1 Introduction

Many real complex systems display the coexistence of more than two attractors corresponding to the long-term behavior in phase space. In addition to a bistable system which displays the positive role of noise in the form of stochastic and coherence resonances [85, 86], a system with multiple coexisting attractors subject to stochastic modulation can exhibit other interesting features, such as noise-enhanced multistability [87], noise-induced preference of attractor [88, 89, 90], noise-induced resonances [29], etc. Noise in such a multistable system provokes a competition between different attracting states; as the system seeks a regular motion in the neighborhood of one attractor, we can see it jumping among the different states [91, 90]. This phenomenon, often called *attractor hopping* [92] is closely related to chaotic itinerancy [93], that has already been observed experimentally [94, 95], showing the alternate motion between fully developed chaos and an ordered behavior. Chaotic itinerancy is often observed in high-dimensional systems such as globally coupled maps [96] and networks of neuronal oscillators [97]. The noise-induced attractor hopping is different from the low-dimensional ordered motion in chaotic itinerancy because the latter takes place

between stable and unstable manifolds and therefore involves a saddle point. A particular case of attractor hopping in a bistable system, two-state on-off intermittency [98], has been observed experimentally in a laser [99]. Both feedback and nonfeedback techniques have been suggested to control such an intermittent behavior [100]. Noise-induced selectivity for certain attractors was studied in Refs. [91, 101, 88, 89]. Recently, Kraut and Feudel [92] showed that in contrast to a bistable system, attractor hopping in a multistable system depends on the structure of the chaotic saddles separating the attractors.

In spite of a large number of theoretical papers devoted to noise-induced switches between multiple states, there has not been to our knowledge a previous experimental report on this phenomenon. In this chapter is studied and shown what we think is the first experimental observation of noise-induced attractor hopping in a fiber laser with multiple coexisting attractors [25]. The attractor hopping manifests itself as *multistate intermittency* and requires the coexistence of multiple invariant subspaces. In a multistable system, noise destabilizes the coexisting states and converts the multistable system into a metastable one. Multiple states that were stable without noise become unstable when noise is applied, giving birth to a new attractor: an intermittency state. As the noise amplitude is increased, the number of the coexisting attractors decreases, as they get involved in the hopping dynamics. It is in this sense that noise allows multistability control.

3.2   Experiment

The experimental setup is the same used in chapter two (Fig. 2.1) and similar to those already described by some authors [24, 78, 80]. The experiments are carried out with a Fabry-Perot cavity 1560-nm erbium-doped fiber laser. The laser is

subjected to the harmonic modulation of a diode pump 976-nm laser. Such a laser has various applications and is commonly used in many laboratories. This laser displays a very rich dynamics that has extensively been studied theoretically [80, 102] and experimentally [24, 78, 80, 23]. The 1.5-m laser cavity is formed by an active heavily-doped erbium fiber of a 70-cm length and 2.7-μm core diameter and two fiber Bragg gratings with a 1-nm FWHM (full width on half-magnitude) bandwidth, having 91% and 95% reflectivities for the laser wavelength. The fiber laser output power is recorded, after going through a wavelength-division multiplexing coupler, with a photodetector and analyzed with an oscilloscope and a Fourier spectrum analyzer. The diode laser output power depends linearly on the laser diode current. In our experiments the diode current is fixed at $I = 69$ mA corresponding to the pump power $P = 19$ mW. The harmonic signal, $A \sin (2\pi f_m t)$ (A and f_m being the amplitude and frequency of external modulation, respectively) from a signal generator and the additive Gaussian noise $N_{in}\xi$ (N_{in} and ξ being the external noise amplitude and a random generated number, respectively) from a noise generator are both applied simultaneously to the diode pump current.

Without external modulation ($A = 0$) and in the absence of external noise ($N_{in} = 0$), the fiber laser power exhibits small-amplitude oscillations (1-2% of the magnitude of the steady-state power) with an average broadband frequency $f_0 = 30$ kHz of its relaxation oscillations. The appearance of this frequency in the spectrum is due to the diode pump laser internal noise and to the fiber laser spontaneous emission [83]. Figure 5.2 shows codimensional-two bifurcation diagram in the parameter space of the modulation frequency and the external noise amplitude. One can see how more and more attractors are involved in the hopping dynamics within a wider parameter range, as the noise amplitude is increased. Moreover, noise induces periodic orbits, not existent prior to its
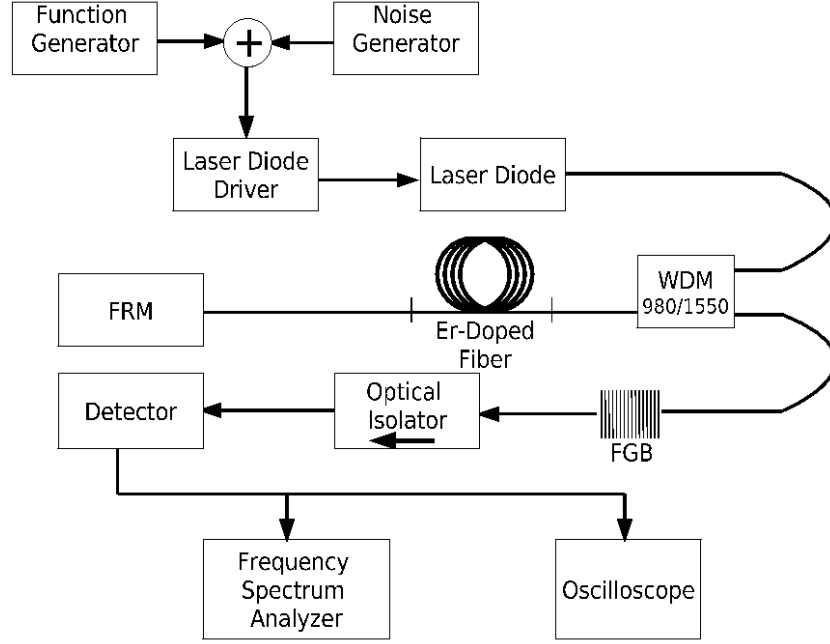
Figure 3.1: Experimental setup.

introduction.

In this work the main interest is in a high-frequency region where the laser exhibits multistability [24]. In Fig. 3.3 we plot the time series and their corresponding power spectra for three coexisting attractors, period 1 (P1), period 3 (P3), and period 4 (P4) when both external modulation with $f_m = 87$ kHz and external noise with amplitude $N_{in} = 0.15$ V are applied. This noise is relatively small, so that no hopping dynamics is observed. As seen in Fig. 3.3(f)], the frequency for P4 is not exactly $f_m/4$ because of nonlinear interaction with f_0 [81].

Switching on and off the signal generator, the laser initial conditions are changed and their corresponding coexisting regimes can be found. For each dynamical regime, the power spectrum displays a different level of frequency-dependent output noise (ground level). One can see that noise has a more pro-
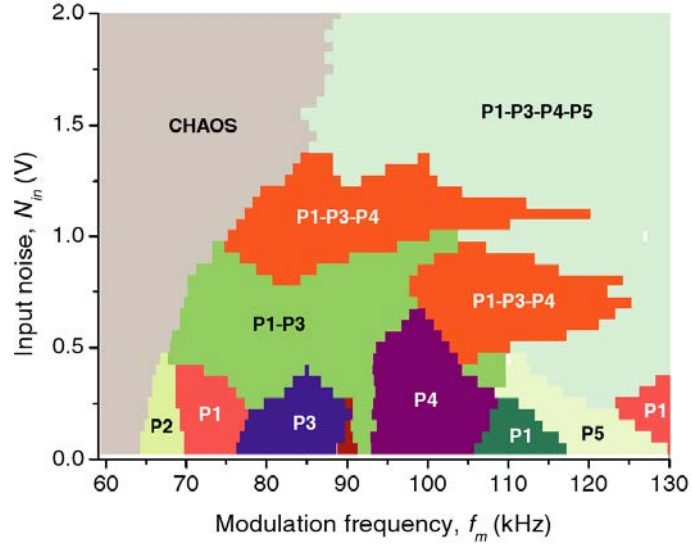
Figure 3.2: Fiber laser state diagram in modulation frequency and noise amplitude parameter space. Different colors stand for different periodic and intermittent states.

nounced effect in the P4 regime than in P3, and the lowest output noise occurs for P1. At a relatively low noise amplitude, the fiber laser is in a periodic state determined by the initial conditions. For instance, if the laser starts with the initial conditions corresponding to P3, it will remain in this state for an infinitely long time showing noisy oscillations with frequency $f_m/3$ [Fig. 3.3(b)]. As the input noise amplitude is increased, the ground level for each attractor also increases until a certain noise threshold is reached and the laser starts jumping back and forth from P3 oscillations to P1, as shown in Fig. 5.3(a). The number of periodic states among which the laser jumps depends on the noise amplitude. In a multistate intermittent regime, the trajectory visits more than two periodic states [Figs. 3.4(b) and 3.4(c)]. When the noise amplitude is large enough, all states are mixed and no structure can be recognized in the trajectory. It is interesting that relatively strong noise can induce higher-periodic orbits that were not there for low noise. For example, period-5 windows appear only when $N_{in} > 1.3$
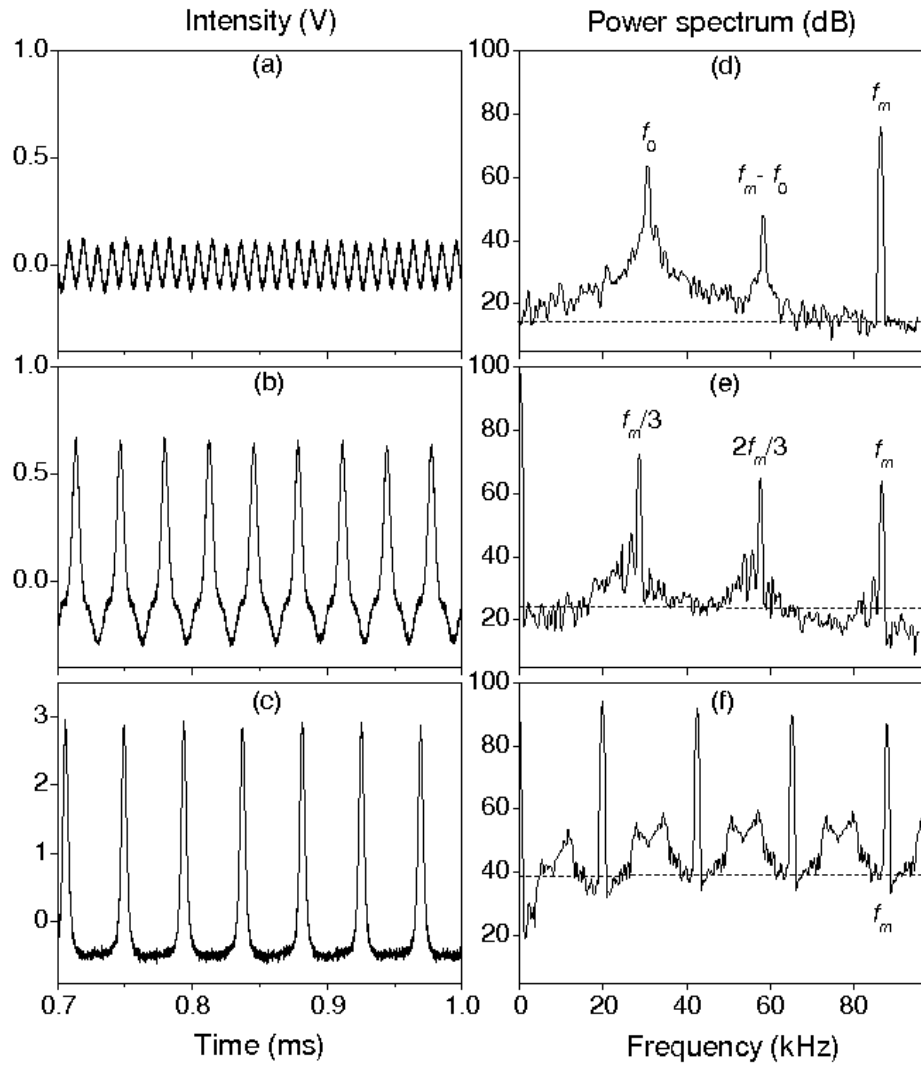
Figure 3.3: (a-c) Time series and (d-f) power spectra of the laser intensity for coexisting (a,d) period-1, (b,e) period-3, and (c,f) period-4 regimes when an external noise $N_{in} = 150$ mV is applied. The horizontal dashed lines indicate the noise level at the modulation frequency $f_m = 87$ kHz. Note the difference in the intensity scale in Fig. 3.3(c).

V [Fig. 3.4(c)].

With the aim of studying characteristic properties of hopping dynamics in mind, we address the following question, how does output noise depend on input noise? Figure 3.5(a) shows, for different coexisting attractors, the dependence of the average output noise N_{out} taking at the modulation frequency f_m of the power spectrum, on the input noise amplitude N_{in}. The three attractors coexistence is observed only for relatively low external noise ($N_{in} < 0.2$ V). For each coexisting state (P1, P3, and P4), the output noise spectral component can be approximated by a lineal dependence on the input noise amplitude [solid lines in Fig. 3.5(a)]. The slope of these lines increases as does the orbit's period; the larger the period, the higher the slope. When the input noise amplitude is increased above 0.2 V, P3 and P1 attractors melt into the intermittent P3-P1 attractor apparently keeping the P3 regime slope for noise dependence. When noise again increases above 0.7 V, the laser starts jumping between three periodic states (P3-P1-P4) while the lineal dependence slope almost disappears, showing that the output-input noise dependence is practically lost. The same diminute slope remains when period 5 takes part in the hopping dynamics (P3-P1-P4-P5). It is only for very strong input noise that all periodic states are mixed and the output noise increases again with the P1 attractor's slope. Since the graphs in Fig. 3.5(a) are in a semilog scale, the straight lines actually represent exponential dependences. This means that the output noise giving in V can be approximated by $N_{out}(V) \sim \exp(\lambda_i N_{in})$, where λ_i is the scaling exponent of the i-periodic orbit. We find $\lambda_1 = 1.54$, $\lambda_3 = 4.52$, and $\lambda_4 = 15.89$, whereas for the hopping attractor $\lambda_{3-1-4} = 0.20$, i.e. it is smaller than λ_1 by a factor of 7.7. This *noise saturation effect* could be useful to design noise-insensitive detectors or for communications with multistable systems.
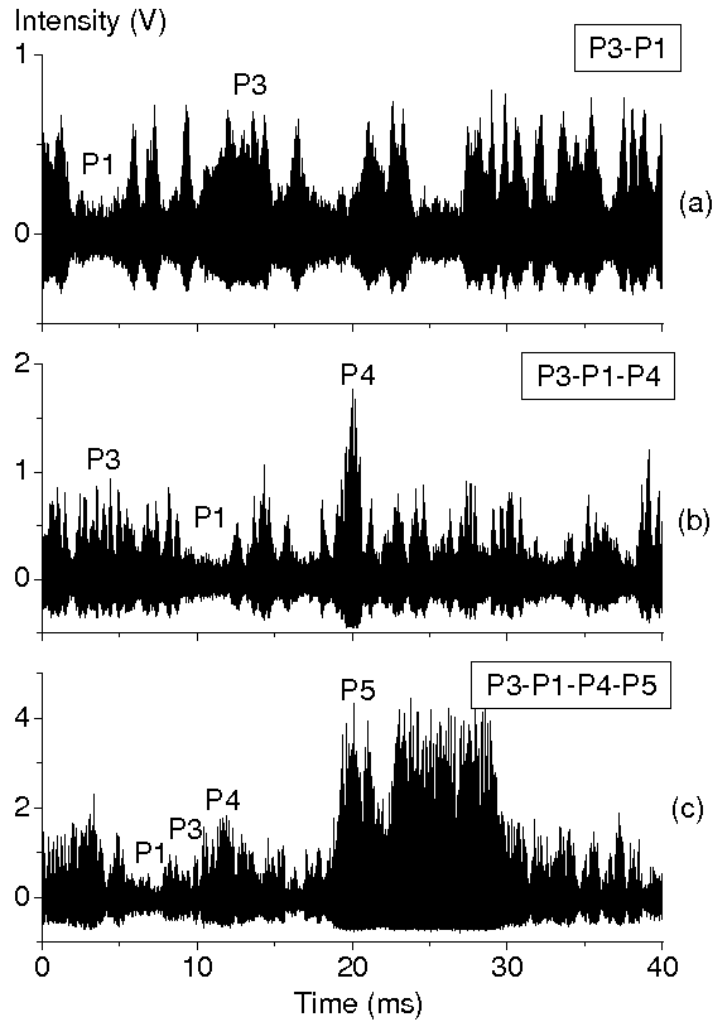
Figure 3.4: Time series in hopping dynamics involving (a) two periodic orbits (P3 and P1) at $N_{in} = 0.5$ V, (b) three periodic orbits (P3, P1, and P4) at $N_{in} = 0.9$ V, and (c) four periodic orbits (P3, P1, P4, and P5) at $N_{in} = 1.5$ V. Note the difference in the intensity scales.
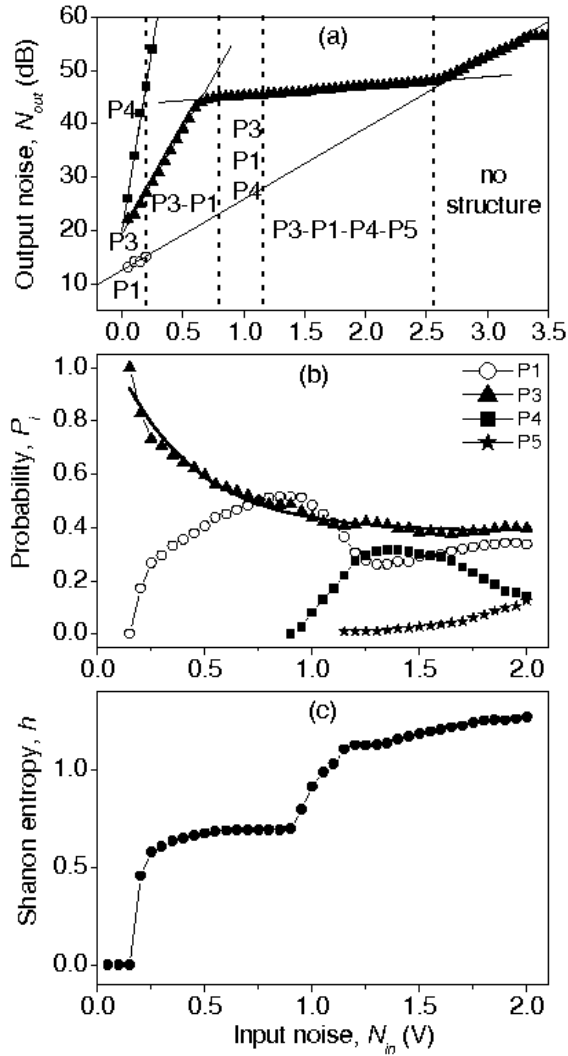
Figure 3.5: (a) Average output noise versus input noise for three coexisting attractors and intermittency regimes. The input noise amplitude is given in V (the generator units) and the output noise is measured in dB (the units of the power spectrum analyzer). The dotted lines show the boundaries between different regimes and the solid lines are linear fits of the slopes. The noise saturation effect is clear seen in the middle part of the figure. (b) Probability of visiting different attracting sets calculated by summing the duration of periodic windows in 10 time series for every noise value. The bold line is the exponential decay fit for the period-3 orbit. (c) The Shannon entropy of the symbol sequence as functions of noise.

Similar to other intermittent regimes the hopping dynamics can be characterized by particular scaling laws. To reveal the physical mechanisms responsible for these scaling relations, we use a statistical approach which is often employed in the study of noisy systems. We are now interested in the nonzero transition probability of every periodic orbit to every other periodic orbit, via a transient on a chaotic saddle, i.e. the probability of the trajectory visiting each one of the coexisting periodic states. Figure 3.5(b) shows this probability P_i as a function of the external noise amplitude. In hopping dynamics, the probability of visiting the P3 orbit, P_3 decays exponentially, as N_{in} is increased [bold line in Fig. 3.5(b)]. The best fit yields the value -0.36 for this characteristic exponent. In the contrary, the probability of visiting P1, P_1 grows as N_{in} is bigger and becomes equal to P_3 at $N_{in} = 0.75$ V. It is exactly at this noise value that the output noise curve in Fig. 3.5(a) changes its slope.

Using the same approach as Poon and Grebogi [91], we qualify order and randomness by encoding dynamics into symbolic sequences of n elements in which the trajectory visits the different attracting sets by crossing the chaotic sets in the boundaries. We assign a symbol s_i for every periodic orbit i that appears in the hopping dynamics. In our case, we need up to four symbols in the alphabet, $s_i = 1, 2, 3, 4$. We then calculate the transition probabilities among the attracting sets using the Shannon entropy, in analogy to the Kolmogorov-Sinai entropy [103].

$$h = \lim_{n \to \infty} \frac{H_n}{n} = \lim_{n \to \infty} \frac{1}{n} \left(-\sum_{|S|=n} p(S) \ln p(S) \right), \qquad (3.1)$$

where $S = s_1, s_2, ..., s_n$ denotes a finite symbol sequence, $p(S)$ is the probability of S, and H_n is the block entropy of block length n. Figure 3.5(c) shows the entropy versus input noise estimated from the experimental data using Eq. (3.1).

Every periodic sequence yields a value of 0. The entropy increases rapidly at the bifurcation point when a new regime appears in hopping dynamics and then it is almost constant. The nontrivial time-scalings appearance in the noisy laser is the consequence of the complex interplay between the coherent and random structures. The horizontal plateau in Fig. 3.5(c) indicates the existence of a certain coherent structure in the set of all possible symbol sequences.

The bifurcation responsible for the jumps between different periodic states can be considered as a kind of crisis and hence the process can be characterized by scaling laws for the characteristic lifetimes [104]. From the experimental data we estimate the mean escape time $\langle T_i \rangle$ for the trajectory to leave the neighborhood of the period-i attracting set as a function of the noise amplitude excess $N_{in} - N_i$ (N_i being the threshold noise value for period i to appears in hopping dynamics). Figure 3.6(a) shows these dependences for different attracting sets. For the period 1 the mean time $\langle T_1 \rangle$ can be well fitted by the exponential decay with noise (bold line); however for other periods, the dynamics is very different, for instance, $\langle T_5 \rangle$ increases with noise and has a maximum at $N_{in} - N_5 \approx 200$ mV. Another interesting quantity of hopping dynamics to investigate is the probability distribution $P(\tau)$ for the length τ of the periodic windows sequence.

For the P1 windows in the two-state intermittency regime between P3 and P1, we find that $P(\tau)$ obeys the universal scaling law for on-off (or two-state on-off) intermittency [105] to be $P(\tau_1) \sim \tau_1^{-3/2}$. When noise is small enough, so that only two periodic regimes are involved in the hopping dynamics, this scaling relation is independent of it. Unfortunately, our experimental data did not allow us to evaluate any scaling relationship for multistate intermittency. We should note that attractor hopping can only be observed for intermediate noise amplitudes. If noise is too weak, the time between two subsequent jumps
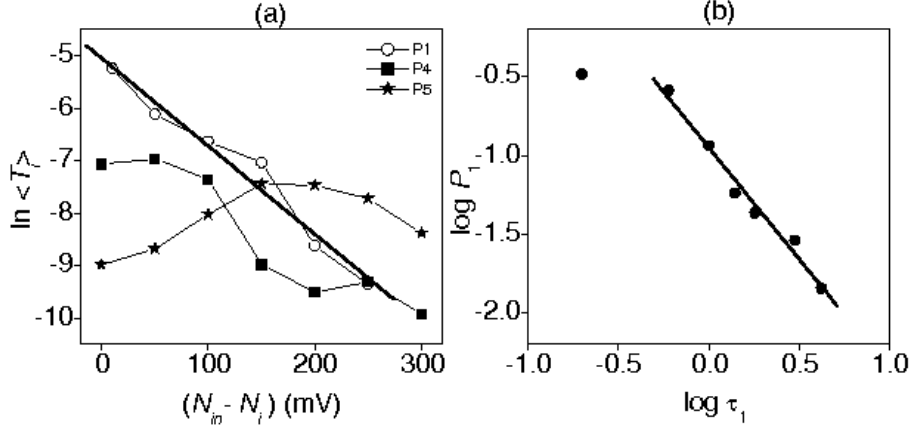
Figure 3.6: (a) Mean escape times $\langle T_i \rangle$ for different attracting sets as a function of the excess of the noise amplitude over the critical value N_i at the onset of intermittency for the period-i state. $N_{1,4,5} = 190, 800, 1150$ mV. (b) Scaling of the probability distribution for period-1 windows inside the intermittent P3-P1 regime showing the -3/2 power law (straight line) for $N_{in} = 200$ mV.

from one state to the other can be arbitrarily large, and if noise is too strong, the attracting sets are no longer recognizable and the whole dynamics obeys a diffusive motion over the entire state space. This change in the behavior as noise increases was studied using finite time Lyapunov exponents. For very small noise strengths, the Lypunov exponent distribution exhibits a pronounced maximum corresponding to the regular motion, but for larger noise strengths it becomes a Gaussian distribution with a maximum at higher Lypunov exponent values [90].

3.3   Conclusions

In this chapter experimentally noise-induced hopping dynamics in a multistable system is characterized. A study of a diode-pumped erbium-doped fiber laser with coexisting periodic attractors is carried out. Under additive noise applied to the

diode pump current the laser displays hopping dynamics. The hopping between two periodic states is characterized by the -3/2 power law for the probability distribution of laminar phase versus laminar length near the onset of intermittency, typical of a two-state on-off intermittency. When the noise amplitude is increased, the number of periodic orbits involved in the hopping dynamics goes up. The average lengths of laminar phases during which the trajectory is in the neighborhood of a particular periodic state varies irregularly depending on the noise amplitude. The character of this dependence is determined by a particular state. The laminar phase can either decrease or increase as the noise amplitude increases resulting in a surprising noise saturation effect, when the output noise of the intermittent state is almost independent of the input noise. Such robustness of the system against external noise could be useful for some applications, for example, in communications with multistable systems or for designing noise-insensitive detectors.

General conclusions

In this dissertation work we performed a systematic experimental study of deterministic and stochastic dynamics of an Erbium doped fiber laser under harmonic modulation applied to the diode-pumped current.

EDFL under pump modulation displays a very rich dynamics including the coexistence of different periodical states. Two new phenomena have been investigated in details. These are pre-bifurcation noise amplification and attractor hopping.

The former phenomenon manifests itself as follows. When a laser parameter is changed so that the laser approaches a bifurcation point, noise increases crucially and the attractor disappears just in the bifurcation point.

The latter phenomenon is the result of noise-induced multistate intermittency, so-called attractor hopping. When noise is added to the system, each one of the involved periodic states mixes on a new intermittent state. In order to understand this stochastic dynamics, a statistical study has been done showing nontrivial scaling relations.

The results obtained in this work may have important applications in natural systems, e.g. geological, biological, medical, and climatological, as well as to develop noise-insensitive sensors.

References

[1] F.T. Arecchi, R. Meucci, G. Puccioni, and J. Tredicce. *Phys. Rev. Lett.*, 49:1217, 1982. 1.1, 1.3, 1.6, 1.7.2

[2] H. Haken. *Advanced Synergetics*. 1983. 1.1, 1.4.2

[3] C. O. Weiss, A. Godone, and Olafsson. *Phys. Rev. A*, 28:369, 1983. 1.1

[4] K. Tanii, M. Tachikawa, M. Kajita, and T. Shimizu. *J. Opt. Soc. Am.*, B5:24–28, 1988. 1.1

[5] F. Mrugala and P. Peplowski. *Z. Phys.*, 38B:359, 1980. 1.1

[6] H. Haken. *Phys. Lett.*, 53A:77, 1975. 1.2

[7] E. N. Lorenz. *J. Atmos. Sci.*, 20:130, 1963. 1.2, 1.2

[8] B. Mandelbrot. *The Fractal Geometry of Nature*. New York, 1977. 1.2, 1.5.2

[9] Kiel L. Douglas and Elliott Euel W. *Chaos Theory in the Social Sciences*. 1997. 1.2

[10] E. Ott. *Chaos in Dynamical Systems*. 1993. 1.2, 1.7.2

[11] F. T. Arecchi, G. L. Lippi, G. P. Puccioni, and J. R. Tredicce. 1.3, 1.3

[12] C. O. Weiss and R. Vilaseca. *Dynamics of Lasers*. Federal Republic of Germany, 1991. 1.3, 1.7.2

[13] J. P. Eckmann. 1.3, 1.7.2

[14] H. Haken. *Synergetics. An Introduction*, volume 3. 1985. 1.4.2

[15] J. Guckenheimer and P. Holmes. *Nonlinear Oscillations Dynamical Systems and Bifurcations of Vector Fields*, volume 68. 1983. 1.5.1

[16] J.-P. Eckmann and D. Ruelle. *Ergodic theory of chaos and strange attractors*, volume 57. 1985. 1.5.1

[17] M. W. Hirsch and S. Smale. *Differential equations dynamical systems and linear algebra*. 1974. 1.5.2

[18] P. Bergé, Y. Pomeau, and C. Vidal. *L'ordre dans le chaos; Order within chaos*, volume 68. 1984. 1.5.2

[19] W. Lauterborn and R. Steinhoff. *J. Opt. Soc Am. B*, 5:1097, 1988. 1.6

[20] J. M. Saucedo-Solorio, A. N. Pisarchik, A. V. Kir'yanov, and V. Aboites. *J. Opt. Soc. Am. B*, 20:490, 2003. 1.6

[21] H. Hohl van der Linden, R. Roy, G. Goldsztein, F. Broner, and S. Strogatz. *Phys. Rev. Lett.*, 74:2220, 1996. 1.6

[22] S. Wieczorek, T. Simpson B. Krauskopf, and D. Lenstra. *Phys. Rev. E*, 65:045207R, 2002. 1.6

[23] R. J. Reategui, A. V. Kir'yanov, A. N. Pisarchik, Y. O. Barmenkov, and N. N. Il'ichev. *Laser Physics*, 14:1277, 2004. 1.6, 2.2, 2.2.2, 2.3.1, 2.3.2, 3.2

[24] A. N. Pisarchik, Y. O. Barmenkov, and A. V. Kir'yanov. *IEEE J. Quantum. Electron.*, 39:1567, 2003. 1.6, 2.2, 2.2.2, 2.3.2, 3.2, 3.2

[25] G. Huerta-Cuellar, A. N. Pisarchik, and Y. O. Barmencov. *Phys. Rev. E*, 78:035202R, 2008. 1.6, 3.1

[26] R. Lang and K. Kobayashi. *IEEE J. Quantum Electron*, 16:347–355, 1980. 1.6

[27] C. Masoller and N. Abraham. *Phys. Rev. A*, 57:1313, 1998. 1.6

[28] Krauskopf B. *Trends in Dynamical Systems*. Handelingen van de Koninklijke Vlaamse Academie van Belgie, 2006. 1.6

[29] C. Masoller. *Phys. Rev. Lett.*, 88:034102, 2002. 1.6, 3.1

[30] T. Baer. *J. Opt. Soc. Am. B*, 49:1217, 1986. 1.6

[31] K. Pyragas, F. Lange, T. Letz, J. Parisi, and A. Kittel. *Phys. Rev. E*, 61:3721, 2000. 1.6

[32] A. N. Pisarchik and B. K. Goswami. *Phys. Rev. Lett.*, 84:14236, 2000. 1.6

[33] A. N. Pisarchik. *Phys. Rev. E*, 64:046203, 2001. 1.6

[34] A. N. Pisarchik, Y. O. Barmenkov, and A. V. Kir'yanov. *Phys. Rev. E*, 68:066211, 2003. 1.6

[35] D. J. Biswas and Harrison R. G. *Phys. Rev. A*, 32:3835, 1985. 1.7.2

[36] Y. Pomeau and P. Manneville. *Comm. Math. Phys.*, 74:189, 1980. 1.7.2

[37] E. A. Spiegel. *Ann. N.Y. Acad. Sci.*, 617:305, 1981. 1.7.2

[38] H. Fujisaka, H. Kamifukumoto, and M. Inoue. *Prog. Theor. Phys.*, 69:333, 1982. 1.7.2

[39] E. Brun, B. Derighetti, D. Meier, R. Holzner, and M. Ravani. *J. Opt. Soc. Am. B*, 2:156, 1985. 1.7.2

[40] D. Dangoisse, P. Glorieux, and D. Hennequin. *Phys. Rev. Lett.*, 57:2657, 1986. 1.7.2

[41] D. J. Biswas, V. Dev, and U. K. Chatterjee. *Phys. Rev. A*, 35:456, 1987. 1.7.2

[42] J. Sacher, W. Els´asser, and E. O. G´obel. *Phys. Rev. Lett.*, 63:2224, 1989. 1.7.2

[43] D. Y. Tang, J. Pujol, and C. O. Weiss. *Phys. Rev. A*, 44:R35, 1991. 1.7.2

[44] W. L. Ditto, S. Rauseo, R. Cawley, G. H. Grebogi, C. Hsu, E. Kostelich, E. Ott H. T. Savage, R. Segnam, M. L. Spano, and J. A. Yorke. 63:923, 1989. 1.7.2

[45] A. N. Pisarchik and V. J. Pinto-Robledo. *Phys. Rev. E*, 66:027203, 2002. 1.7.2

[46] A. Einstein. *Investigations on the Theory of the Brownian Movement.* New York, 1956. 1.8

[47] Jian-Quiao Sun. Stochastic dynamics and control. page 411, 2006. 1.8

[48] Thomas Wellens, Vyacheslav Shatokhin, and Andreas Buchleitner. *Rep. Prog. Phys.*, 67:45–105, 2004. 1.8.1

[49] H. Kramers. *Physica (Utrecht)*, 7:284, 1940. 1.8.1

[50] G. P. Agrawal. *Fiber optic communication systems.* New York, 2002. 1.9

[51] M. J. F. Diginnet. *Rare Earth Doped Fiber Lasers and Amplifiers.* New York, 1993. 1.9, 2.2

[52] A. Bjarklev. *Optical fiber amplifiers: design and system aplications.* Boston. 1.9

[53] E. Desurvire. *Erbium doped fiber amplifiers.* New York, 1994. 1.9

[54] G. P. Agrawal. *Applications of nonlinear fiber optics.* San Diego, CA, 2001. 1.9

[55] C. R. Giles and E Desurvire. *J. Lightwave Technology*, 9:271, 1991. 1.9

[56] A. A. L. Saleh, R. M. Jopson, J. D. Evankow, and J. Aspell. *IEEE Photon Technol. Lett.*, 2:714, 1990. 1.9

[57] B. Pedersen, A. Bjarklev, O. Lumholt, and J. H. Povlsen. *IEEE Photon Technol. Lett*, 3:548, 1991. 1.9

[58] T. Georges, E. Delevaque, and M. Monerie. Optical amplifiers and their applications. *OSA Technical Digest Series*, 17:WE4, 1992. 1.9

[59] P. F. Wysocki, J. L. Wagener, M. J. F. Digonnet, and H. J. Shaw. *Proc. Soc. Photo-Opt. Instrum. Eng.*, 66:1789, 1993. 1.9

[60] S. A. Akhmanov, Y. E. D'yakov, and A. S. Chirkin. *Introduction to Radio-physics and Optics (in Russian)*. Moscoe. 2.1

[61] A. V. Fedorov, S. L. Harper, S. G. Philander, B. Winter, and A. Wittenberg. *Bull. Am. Meteorol. Soc.*, 84:911, 2003. 2.1

[62] D. Chen, M. A. Cane, A. Kaplan, S. E. Zabiak, and D. Huang. *Nature*, 428:733, 2004. 2.1

[63] J. V. Greenman and T. G. Benton. *The Americal Naturalist*, 161:225, 2003. 2.1

[64] E. Surovyatkina. Nonlinear processes en geophysics. 12:25, 2005. 2.1

[65] D. Alonso, A. J. McKane, and M. Pascual. *J. R. Soc. Interface*, 4:575, 2007. 2.1

[66] J. García-Ojalvo and R. Roy. *Phys. Lett. A*, 224:51, 1996. 2.1

[67] H. Lamela, S. Pérez, and G. Carpintero. *Opt. Lett.*, 26:69, 2001. 2.1

[68] K. Wiesenfeld. *J. Stat. Phys.*, 38:1071, 1885. 2.1

[69] K. Wiesenfield and B. McNamara. *Phys. Rev. A*, 33:629, 1986. 2.1, 2.2.2, 2.2.2

[70] R. Corbalán, J. Cortit, A.N. Pisarchik, V. N. Chizhevsky, and R. Vilaseca. *Phys. Rev. A*, 51:663, 1995. 2.1, 2.2.2, 2.2.2

[71] G. Huerta-Cuellar, A. N. Pisarchik, A. V. Kir'yanov, Y. O. Barmencov, and J. del Valle Hernandez. *Phys. Rev. E*, 79:036204, 2009. 2.1

[72] Y. A. Kravtsov, S. G. Bilchinskaya, O. Y. Butkovskii, I. A. Rychka, and E. D. Surovyatkina. *Zh. Eksp. Teor. Fiz.; JETP 93*, 120:1527; 1323, 2001; 2001. 2.1

[73] Y. A. Kravtsov and E. D. Surovyatkina. *Phys. Lett. A*, 319:348, 2003. 2.1

[74] E. D. Surovyatkina. *Phys. Lett. A*, 329:169, 2004. 2.1

[75] E. D. Surovyatkina, Y. A. Kravtsov, and J. Kurths. *Phys. Rev. E*, 72:046125, 2005. 2.1

[76] C. Jeffries and K. Wiesenfeld. *Phys. Rev. A*, 31:1077, 1985. 2.1

[77] J. M. Saucedo-Solorio, A. N. Pisarchik, A. V. Kir'yanov, and V. Aboites. *J. Opt. Soc. Am. B*, 20:490, 2003. 2.2, 2.2.2

[78] A. N. Pisarchik, Y. O. Barmenkov, and A. V. Kir'yanov. *Phys. Rev. E*, 68:066211, 2003. 2.2, 2.2.2, 2.3.2, 3.2

[79] A. N. Pisarchik, Y. O. Barmenkov, and A. V. Kir'yanov. volume 94. 2004. 2.2, 2.2.2, 2.3.1, 2.3.2

[80] A. N. Pisarchik A. V. Kir'yanov Y. O. Barmenkov and R. Jaimes-Reátegui. *J. Opt. Soc. Am. B*, 22:2107, 2005. 2.2, 2.2.2, 3.2

[81] A. N. Pisarchik and Y. O. Barmenkov. *Opt. Commun.*, 254:128, 2005. 2.2, 2.2.2, 2.3.1, 2.3.2, 3.2

[82] F. T. Arecchi and R.G. Harrison. *Instabilities and Chaos in Quantum Optics.* New York, 1987. 2.2

[83] Y. O. Barmenkov and A. V. Kir'yanov. *Optics Express*, 12:3171, 2004. 2.2.1, 2.3.1, 3.2

[84] Auger up-conversion is a noticeable factor for edf with high concentration of er^3+ ions in the presence of er^3+-er^3+ pair clusters. 2.2.1, 2.3.1

[85] L. Gammaitoni, F. Marchesoni, and S. Santucci. *Phys. Rev. Lett.*, 74:1052, 1995. 3.1

[86] A. S. Pikovsky and J. Kurths. Coherence resonance in a noise-driven excitable system. *Phys. Rev. Lett.*, 78:775, 1997. 3.1

[87] S. Kim, S. H. Park, and C. S. Ryu. *Phys. Rev. Lett.*, 78:1616, 1997. 3.1

[88] K. Kaneko. *Phys. Rev. Lett.; Physica D (Amsterdam)*, 78; 124:2736; 322, 1997; 1998. 3.1

[89] K. Kaneko. *Physica D (Amsterdam)*, 124:322, 1998. 3.1

[90] S. Kraut, U. Feudel, and C. Grebogi. *Phys. Rev. E*, 59:5253, 1999. 3.1, 3.2

[91] L. Poon and C. Grebogi. *Phys. Rev. Lett.*, 75:4023, 1995. 3.1, 3.2

[92] S. Kraut and U. Feudel. *Phys. Rev. E*, 66(R):015207, 2002. 3.1

[93] K. Ikeda, K. Matsumoto, and K. Otsuka. *Prog. Theor. Phys. Suppl.*, 99:295, 1989. 3.1

[94] F. T. Arecchi, G. Giacomelli, P. L. Ramazza, and S. Residori. *Phys. Rev. Lett.*, 65:2531, 1990. 3.1

[95] W. Wang, I. Kiss, and J. Hudson. Experiments on arrays of globally coupled chaotic electrochemical oscillators: Synchronization and clustering. *Chaos*, 10:248, 2000. 3.1

[96] K. Kaneko. *Physica D*, 41:137–172, 1990. 3.1

[97] M. Timme F. Wolf and T. Geisel. *Phys. Rev. Lett.*, 89:154105, 2002. 3.1

[98] Y.-C. Lai and C. Grebogi. *Phys. Rev. E*, 52R:3313, 1995. 3.1

[99] A. N. Pisarchik and V. J. Pinto-Robledo. *Phys. Rev. E*, 66:027203, 2002. 3.1

[100] Y. Nagai, X.-D. Hua, Y.-C.Lai; R. J. Reategui, and A. N. Pisarchik. *Phys. Rev. E; ibid*, 54; 69:1190; 067203, 1996; 2004. 3.1

[101] Y.-C. Lai. *Phys. Lett. A*, 221:375, 1996. 3.1

[102] I. J. Sola, J. C. Martín, and J. M. Álvarez. *Optics Communications*, 258:59, 2006. 3.2

[103] A. N. Kolmogorov; Ya. G. Sinai. *Dok. Acad. Nauk SSSR; ibid.*, 119; 124:861; 768, 1958; 1959. 3.2

[104] E. Ott. *Chaos in Dynamical Systems*. Cambridge UK, 1993. 3.2

[105] J. F. Heagy, N. Platt, and S. M. Hammel. *Phys. Rev. E*, 49:1140, 1994. 3.2